

2023-05-01

Structure Study Of Small Heat Shock Protein 27

Zhaobo Li
University of Texas at El Paso

Follow this and additional works at: https://scholarworks.utep.edu/open_etd



Part of the [Chemistry Commons](#)

Recommended Citation

Li, Zhaobo, "Structure Study Of Small Heat Shock Protein 27" (2023). *Open Access Theses & Dissertations*. 3880.

https://scholarworks.utep.edu/open_etd/3880

This is brought to you for free and open access by ScholarWorks@UTEP. It has been accepted for inclusion in Open Access Theses & Dissertations by an authorized administrator of ScholarWorks@UTEP. For more information, please contact lweber@utep.edu.

STRUCTURE STUDY OF SMALL HEAT SHOCK PROTEIN 27

ZHAOBO LI

Master's Program in Chemistry

APPROVED:

Ricardo A. Bernal Ph.D., Chair

Zacariah L Hildenbrand, Ph.D.

Eda Koculi, Ph.D.

Anita Quintana, Ph.D.

Stephen L. Crites, Jr., Ph.D.
Dean of the Graduate School

Copyright ©

By

Zhaobo Li

2023

Dedication

To my family

STUCTURE STUDY OF SMALL HEAT SHOCK PROTEIN 27

by

ZHAOBO LI

THESIS

Presented to the Faculty of the Graduate School of

The University of Texas at El Paso

in Partial Fulfillment

of the Requirements

for the Degree of

MASTER OF SCIENCE

Department of Chemistry and Biochemistry

THE UNIVERSITY OF TEXAS AT EL PASO

MAY 2023

Abstract

Molecular chaperones are a class of oligomeric proteins that play a critical role in preventing the aggregation of non-native protein so that these proteins can later be refolded. Chaperones are ubiquitously expressed in all the kingdoms of life where their function is to counteract cellular stress and to maintain protein homeostasis. One subgroup of molecular chaperones is characterized by low molecular weight and are termed small heat shock proteins. The focus of the proposed research is the small heat shock protein 27 (Hsp27). Hsp27 is an ATP independent chaperone that is overexpressed in response to heat shock, radiation damage, oxidative damage, or other cellular stress in order to preserve protein homeostasis. Notably, there is an oligomeric reshuffling of Hsp27 from large oligomers to functional dimers under stressful conditions. Phosphorylation at three serine residues, 15, 78, 82 initiate the dynamic equilibrium change from large oligomeric complexes to much smaller dimeric subunits.

Accumulation of misfolded protein causes numerous diseases that impacts the daily life of millions of individuals. For example, the misfolding or aggregation of microtubule associated protein Tau, and neuron associated alpha-synuclein are the pathological hallmarks for Alzheimer's and Parkinson disease, respectively. Studies have suggested a significant role of Hsp27 in inhibiting the aggregation of both Tau and alpha-synuclein. The contact area between Hsp27 and its client proteins Tau and alpha-synuclein has been characterized by a variety of biophysical techniques that enhance our understanding neurotherapeutics. However, a high-resolution atomic structure of the monomeric full length Hsp27 still remains ambiguous because of the struggles in obtaining a homogeneous purified product for reconstruction and by the fact that the protein has intrinsic disorder. This intrinsic disorder is a functional attribute of a large portion of the N-terminal and C-terminal regions. This project aims to apply cryo-EM 3D

reconstruction techniques to elucidate a high-resolution structure of human Hsp27 in complex with its substrates Tau and alpha-synuclein with the idea that the association with substrate will stabilize previously disordered regions in Hsp27.

Table of Contents

Dedication	iii
Abstract	v
Table of Contents	vii
List of Figures	ix
Chapter 1: Protein Folding and Small Heat Shock Protein 27.....	1
1.1 Protein Folding and Molecular Chaperone	1
1.2 Small Heat Shock Protein 27	2
1.3 Substrate Neuronal Protein Tau	4
1.4 Substrate Neuronal Protein Alpha Synuclein	6
1.5 Project Goal and Hypothesis.....	10
Chapter 2: Molecular Cloning	11
2.1 Background of Molecular Cloning	11
2.2 Material and Method.....	14
2.3 Result	17
2.4 Discussion	18
Chapter 3: Recombinant Protein Expression	19
3.1 Background of Recombinant Protein Expression	19
3.2 Material and Method.....	22
3.3 Result	28
3.4 Discussion	34
Chapter 4: Protein Chromatography Purification	36
4.1 Background of Protein Chromatography	36
4.2 Material and Method.....	40
4.3 Result	43
4.4 Discussion	50
Chapter 5: Structural and Biophysical Characterization.....	52
5.1 Background	52
5.2 Material and Method.....	56

5.2.1 Alpha Synuclein Aggregation Assay	56
5.2.2 Tau Fiber Formation Assay	56
5.2.3 DLS Measurement	57
5.2.4 Hsp27 Fiber Complex Assemble Assay	57
5.3 Result	58
5.4 Discussion	62
5.5 Future Direction	63
References	64
Vita	70

List of Figures

Figure 1.1. Cryo-EM atomic model of Tau filament from Alzheimer's brain[30]	6
Figure 1.2. schematic diagram of alpha synuclein interaction with SNARE complex [37]	8
Figure 2.1. 0.7% agarose gel of the PCR amplification end products. Alpha synuclein gene (SNCA) presents as solid bright band between 750 bp and 500bp in the second line. Tau gene (MAPT) presents as bright band slightly above 2000bp and one faint band around 750bp in third line.....	17
Figure 3.1. 10% SDS-PAGE of the human alpha synuclein protein expression conditions. Line 1 protein marker, line 2 uninduced cell sample, line 3 to 5 induced cell sample with solid sharp band around 14.4 kDa.	28
Figure 3.2. 7.5% SDS-PAGE of the human Tau protein expression conditions. Line 1 protein marker, line 2 uninduced cell sample, line 3 to 5 induced cell sample with solid sharp band around 110 kDa.....	29
Figure 3.3. 12.5% SDS-PAGE of the human Hsp27 WT protein expression conditions. Line 1 protein marker, line 2 uninduced cell sample, line 3 induced cell sample with solid sharp band around 27 kDa.....	30
Figure 3.4. 12.5% SDS-PAGE of the human heat shock protein 27 constitutively active serine mutant protein expression conditions. Line 1 protein marker, line 2 uninduced cell sample, line 3 to 5 induced cell sample with solid sharp band around 27 kDa.....	31
Figure 3.5. 7.5% SDS-PAGE of the Tau ammonium sulfate precipitate optimization. Line 1: protein marker. Line 2 resuspended protein pellet at 30% ammonium sulfate. Line 3: supernatant at 30% ammonium sulfate saturation. Line 4: resuspended protein pellet at 35% ammonium sulfate. Line 4: supernatant at 35% ammonium sulfate saturation. Line 5: supernatant at 35% ammonium sulfate saturation. Line 6: resuspended protein pellet at 40% ammonium sulfate precipitation. Line 6: supernatant at 40% ammonium sulfate saturation. Line 7: resuspended protein pellet at 45% ammonium sulfate precipitation. Line 8: supernatant at 45% ammonium sulfate saturation.	32
Figure 3.6. 12.5% SDS-PAGE of the alpha syncuelin ammonium sulfate precipitate optimization. Line 1: protein marker. Line 2 resuspended protein pellet at 30% ammonium sulfate. Line 3: supernatant at 30% ammonium sulfate saturation. Line 4: resuspended protein pellet at 35% ammonium sulfate. Line 4: supernatant at 35% ammonium sulfate saturation. Line 5: supernatant at 35% ammonium sulfate saturation. Line 6: resuspended protein pellet at 40% ammonium sulfate precipitation. Line 6: supernatant at 40% ammonium sulfate saturation. Line 7: resuspended protein pellet at 45% ammonium sulfate precipitation. Line 8: supernatant at 45% ammonium sulfate saturation.....	33
Figure 4.1. Ion exchange chromatography of Alpha Synuclein	43
Figure 4.2. 12.5 % SDS-PAGE of alpha synuclein fractions from Ion exchange column	44
Figure 4.3. Hydrophobic interaction chromatography of alpha synuclein	44
Figure 4.4. 12.5% SDS-PAGE of fractions from hydrophobic interaction column	45
Figure 4.5. size exclusion chromatography of alpha synuclein	45
Figure 4.6. 12.5% SDS-PAGE of fractions from SEC column	46
Figure 4.7. Ion exchange chromatography of Tau	46
Figure 4.8. 10% SDS-PAGE of fractions from ion exchange column	47
Figure 4.9. size exclusion chromatogram of Tau.....	47
Figure 4.10. 10% SDS-PAGE of fractions from size exclusion column	48

Figure 4.11. Ion exchange chromatogram of Hsp27.....	48
Figure 4.12. 10% SDS-PAGE of fractions from ion exchange column	49
Figure 4.13. Comparison of size exclusion chromatography of Hsp27 WT with Hsp27 triple serine mutant.....	49
Figure 4.14. 12.5% SDS-PAGE of fractions from size exclusion column.....	50
Figure 5.1. Traditional dynamic light scattering schematic diagram.....	53
Figure 5.2. Negative stain image of alpha synuclein fiber	58
Figure 5.3. Negative stain image of heparin induced Tau fiber.....	59
Figure 5.4. DLS analysis of Hsp27 triple serine mutant and Hsp27 WT	60
Figure 5.5. SDS-PAGE of alpha synuclein and Hsp27 triple serine mutant co-sedimentation assay	61

Chapter 1: Protein Folding and Small Heat Shock Protein 27

1.1 PROTEIN FOLDING AND MOLECULAR CHAPERONE

Proteins are one of the most sophisticated biological macromolecules that play a vital role in all cellular functions.[1] In general, proteins must be folded into a proper three-dimensional conformation to attain their biological function.[2] The protein folding process was initially described by Christian Anfinsen denatured ribonuclease refolding experiment. The experiment demonstrated that the denatured ribonuclease was able to independently refold to its native conformation without the participation of other enzymes. [3] Interestingly, protein must maintain a certain degree of structural flexibility in order to interact with numerous substrates. Majority of protein are barely thermodynamically stable under physiological cellular condition.[4] Diverse physiological stressful conditions such as heat and oxidative stress can drastically disrupt protein intermolecular interactions, which consequently lead to loss of protein function.[5] Not surprisingly, misfolding or aggregation of proteins causes detrimental effects in cellular homeostasis that will eventually lead to the progression of various diseases such as type 2 diabetes, and cardiovascular disease.[6] A class of proteins, termed molecular chaperones, usually serve as the cell first line of defense during stressful conditions by interacting with non-native protein to maintain proteostasis to acquire its native conformation. [7] Chaperones can be categorized based on their molecular weight such as heat shock protein 100, heat shock protein 60, heat shock protein 70 as well as small heat shock proteins like Hsp27. These proteins are widely involved in nascent peptide folding, partially denatured protein refolding and prevent protein irreversible aggregation. Both Hsp60 and Hsp70 are able to refold the non-native protein in ATP dependent folding cycle. Hsp70 primarily refolds the nascent synthesized proteins. While

Hsp60 targets for refolding the late stage of protein which is not able to reach thermodynamic favorable state.[8]

1.2 SMALL HEAT SHOCK PROTEIN 27

Small heat shock proteins are ubiquitously expressed in all kingdoms of life and play essential roles in cellular stress response in an ATP independent manner. Humans express 10 different small heat shock proteins that are categorized by their molecule weight.[9] A small heat shock protein's main function is to preserve a misfolded protein in a folding competent state. The misfolded protein can then be transferred to a chaperonin such Hsp60 and its co-chaperonin Hsp10 to be refolded to its native conformation through an ATP dependent hsp60/10 mechanism or Hsp70 protein [10] As the name implies, small heat shock protein 27 is 27 kDa in size and is encoded by the HSBP1 gene. Ironically, Hsp27 is characterized as an intrinsically disordered protein due to its unique architecture where an extremely disordered long amino terminal region and a short flexible carboxyl terminal region flank a central α -crystallin domain (ACD) that is highly conserved in the small heat shock protein family.[11] Hsp27 can form a dimeric complex that is considered the fundamental functional building block that is used to form larger oligomers. The dimer interaction is through hydrogen bonding between monomers to form a beta sheet in the central α -crystallin domain.[12]

The central α -crystalline domain from residues 86-169 is composed of nine beta strands that form two anti-parallel β -sandwich folds which the beta sheet interaction generated between two of these ACD domains modulates the dimerization of small Hsp27. The dimer can then assemble to form an oligomer of up to 900 kDa via interactions across dimers to adjacent dimers using both the amino and carboxy terminal regions which then bind to the ACD domain. [13] Similar to other mammalian small heat shock proteins, Hsp27 can assemble to oligomers of

various sizes that rapidly dissociate to small oligomers and dimers under stress induced phosphorylation.[14]

Protein phosphorylation is evaluated as a quintessential post translational modification in eukaryotic cells. Reversible phosphorylation plays a key role in signal transduction pathways where it serves as a mediator for cells to rapidly respond to both intracellular and intercellular signals.[15] For Hsp27, phosphorylation plays a role in regulating the dynamic equilibrium shift from large oligomeric complexes to dimers and back again. Serine 15 (S15), Serine 78 (S78) and Serine 82 (S82) located in the amino terminus and Threonine 43 (T 143) in the central α -crystallin domain are characterized as the phosphorylation sites in Hsp27 responsible for oligomer disruption. Preliminary research has illustrated that the phosphorylation at Serine (S15), Serine (S78) and Serine (S82) are primarily inducing conformational changes from large oligomeric complexes to dimers.[16] Numerous of kinase are able to phosphorylate Hsp27 such as mitogen activated protein kinase activated protein kinase 2, 3 ,5 (MAPKAPK2, 3, 5). Several research have demonstrated protein phosphatase 2A (PP2A) is able to be dephosphorylated Hsp27 to reform large oligomer complex.[17]

The disordered N-terminal region of Hsp27 is composed of the first 93 amino acids which are predominantly hydrophobic or aromatic amino acid. The WF/EPF motif from residue 16 to 19 has been shown to play a critical role in Hsp27 protein chaperoning activity. The highly conserved N-terminal region has been shown to stabilize high molecular weight oligomers.[18] However, the intrinsic disorder found in the N-terminal region is the primary obstacle for high resolution structure determination. The N-terminal region has been found to bind to non-native substrate protein to achieve its chaperone function. In the non-native conformation, the hydrophobic surface of the substrate protein will be exposed to the aqueous environment. The N-

terminal region of Hsp27 has a tendency to bind to partially denatured protein through the hydrophobic residues found on its surface.[19] Even though partially denatured proteins can bind to the ACD domain, binding the N-terminal region is required to maintaining its chaperone function.[20] The highly conserved ACD domain forms an immunoglobulin like structure that is composed of two β sheets. Beta strands 4, 5 and extended strands 6+7 form one beta-sheet. Another beta sheet is composed of strands 3, 8 and 9. Beta strands 4 and 8 form a hydrophobic groove which is versatile region in charge of substrate binding.

The C terminal region, which contains the last 36 residues, is composed of polar and charged residues. The higher flexibility of this region contributes to the intrinsic disordered characteristics of Hsp27 as well. The IXI/V motif can interact with the β 4 and β 8 groove to facilitate large oligomer formation.[21] The protein interaction between the IXI/V motif and β 4/ β 8 is one of the best characterized protein-protein interactions primarily in charge of oligomer stabilization. This protein-protein interaction drives the association of the flexible IXI motif with the groove between β 4 and β sheet 8.[22]

1.3 SUBSTRATE NEURONAL PROTEIN TAU

Alzheimer disease (AD) is a progressive neurodegenerative disease central nervous system that predominantly affects individuals over 65. Currently, more than 6 million Americans are afflicted from Alzheimer disease. The clinical manifestations include memory loss, cognitive impairment, and disorientation. Despite significant research effort in therapeutic treatment of Alzheimer, it remains an incurable condition that impacts a large population. Preliminary investigation has revealed that the formation of amyloid plaques from beta-amyloid peptide and

neurofibrillary tangles consisting of aberrant hyperphosphorylated microtubule-associated protein tau (Tau) are the pathological hallmarks of Alzheimer disease.[23]

Microtubule-associated protein Tau, which is primarily expressed in neurons and encoded by the MAPT gene, plays a crucial role in stabilizing the microtubules that are integral components of the cytoskeleton, responsible for intracellular transport.[24] However, the abnormal behavior of Tau has been shown to be similar in various neurodegenerative disorders, including Alzheimer's disease. In these disorders, Tauopathy is characterized by the accumulation of insoluble amyloid filaments containing Tau protein, resulting in irreversible damage to neuronal cells.[25]

Human MAPT gene is able to encode 6 isoforms from 352 to 441 amino acids contributed from RNA alternative splicing. [26] The tau can be characterized in three domains which are N terminal projection domain, proline rich domain and microtubule binding domain. The interaction between Tau and microtubule is dynamically modulated by several post translational modifications including phosphorylation, glycosylation, and nitration.[27] Tau aggregation is associated with neurodegenerative disorders and is directly correlated with Tau hyperphosphorylation. The normal level phosphorylation of Tau occurred at several serine or threonine residues and mediates the dynamic binding equilibrium between Tau and microtubular.[28] The normal phosphorylation occurs at different sites for Tau isomers. Hyperphosphorylation leads Tau incompetent to bind to the microtubular, causing the destabilization of microtubular leading the neuron death. The hyperphosphorylated Tau thermodynamically favors the formation of neurofibrillary tangles (NFTS), which has been identified in Alzheimer disease patient.[29] The high atomic resolution of Tau from Alzheimer disease brain sample, determined by cryo-EM, enhances the current understanding of tauopathy.

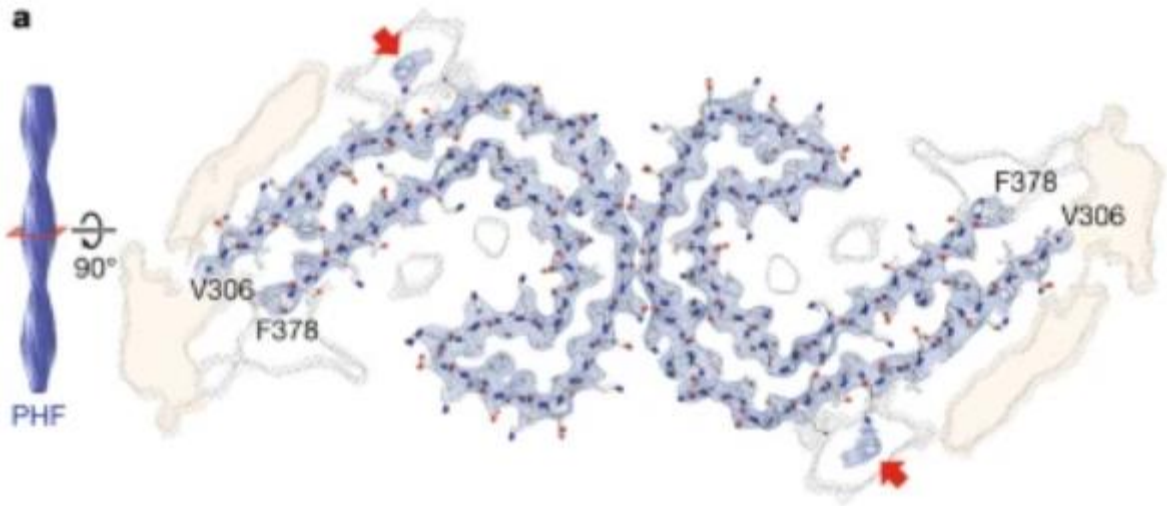


Figure 1.1 Cryo-EM atomic model of Tau filament from Alzheimer's patient brain [30]

Recent studies have shown that Hsp27, a small heat shock protein, is competent to inhibit Tau aggregation both in vitro and in vivo. Hsp27 has been shown to interact with the Tau PHF domain, which is responsible for filament formation, and prevent the aggregation of Tau proteins. Moreover, studies on the truncation of the N-terminus of Hsp27 have indicated that the central ACD alone is insufficient to inhibit Tau filament formation. The N-terminus of Hsp27 has been shown to play a vital role in its chaperone activity, as it is responsible for the oligomerization of Hsp27 and its subsequent interaction with abnormal proteins. This demonstrates the significance of understanding the molecular mechanisms by which Hsp27 interacts with Tau and other client proteins, in order to advance potent therapeutic interventions. [31]

1.4 SUBSTRATE NEURONAL PROTEIN ALPHA SYNUCLEIN

Parkinson disease (PD), a central nervous system neurodegenerative disorder is caused by substantial loss of dopaminergic neurons. Over 95% of cases occurs the people over 55. The

clinical symptoms of Parkinson disease are typically characterized by rigidity, hypophonia and drooling.[32] The primary pathological hallmark of Parkinson disease is Lewy bodies which is composed of various of filament proteins such as alpha synuclein.[33] The toxic alpha synuclein filament is able to disrupt the cell membrane which is able to lead the death of neuron cells. Human alpha synuclein encoded from SNCA gene is a small 14.5 kDa presynaptic protein composed of 140 amino acids. Alpha synuclein can be characterized in three domains. The N terminus (1 to 60 residues) which contains lipid binding motif to interact with neuron cell membrane; the center hydrophobic domain known as NAC and the negative charge, disordered short C terminus.[34] While α -synuclein has been studied extensively over the past few decades, the clear physiological function of α -synuclein in regulating central neurons remains enigmatic.

Alpha synuclein is most abundantly localized in axon terminal in neurons, which plays vital role in modulation of synaptic vesicle transportation.[35] The association between alpha synuclein and synaptic vesicle is mediated by calcium ion binding to C terminus residues. The N terminal membrane binding domain of alpha synuclein is able to bind to phospholipid bilayers of synaptic terminal cell membrane. Preliminary C terminal truncation experiment demonstrates that highly negative charged C terminus plays critical role in association with synaptic receptor protein (SNARE) to facilitate vesicle fusion. [36]

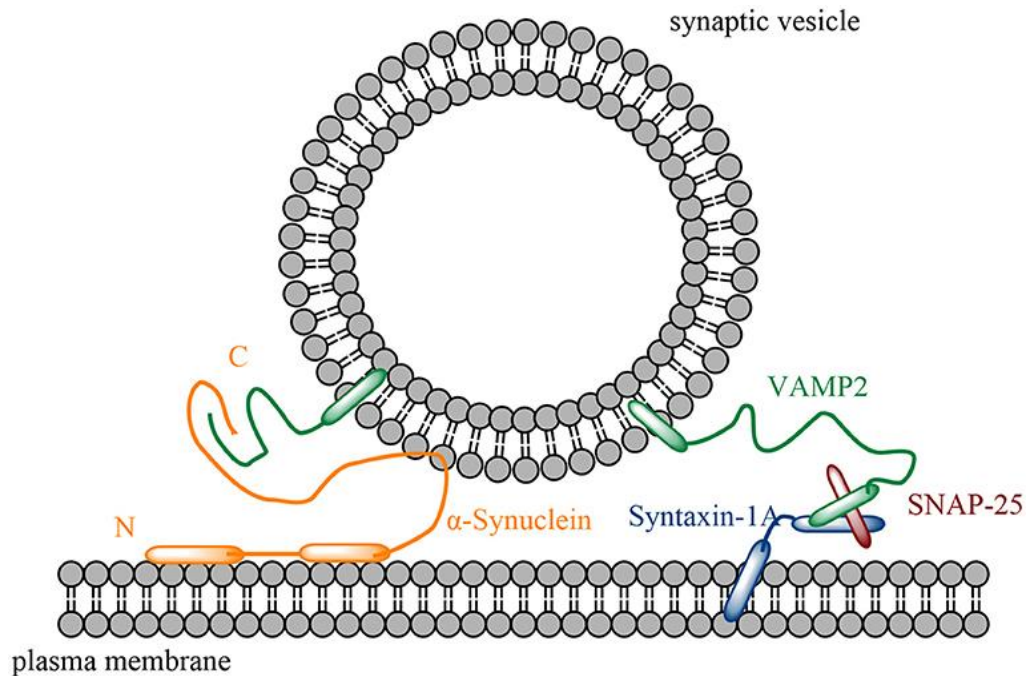


Figure 1.2: schematic diagram of alpha synuclein interaction with SNARE complex [37]

The formation of alpha synuclein to small soluble oligomers and elongated insoluble fibers are extremely detrimental to neuron cell. To date, the alpha synuclein aggregation mechanism is still enigmatic. One proposed model depicts the early stage alpha synuclein fiber growth is nucleation polymerization. Alpha synuclein monomers are able to initially form oligomer through beta-sheet structure. The oligomer can serve as a seeding template competent for self-assembly with the continuous addition of monomer. [38] Several single point mutation of alpha synuclein (A30P, A53T and E46K) have been described to associate with Parkinson Disease. Interestingly, the growth kinetics of each mutant is significantly differed based on in vitro fiber formation study.[39]

The various growth condition such pH and ionic strength can drastically impact aggregation kinetic and mature fiber morphology.[40] This discovery enhances the current understand of fundamental mechanism of alphas synuclein fiber formation. Another bottle neck of alpha

synuclein research is the detailed mechanism of fiber cell-to-cell propagation. Current major hypothesis of alpha synuclein propagation is via exocytosis of aggregates.[41]

The high-resolution atomic structure of alpha synuclein fiber reveal the detail structural information, which shed the light on the advancement of alpha synuclein therapeutics.

Preliminary studies have found that the Hsp27 is able to suppress the alpha synuclein fiber formation in vitro. The sedimentation experiment demonstrated that constitutive active triple serine mutant was able to form a stable complex with α -synuclein fibrils through its intrinsically disordered N-termini. Hsp27 core domain mutant alone was not able to co-sedimented with alpha synuclein, which is indicative of Hsp27 core domain mutant incompetent for stable binding to alpha synuclein fiber. The hydrophobicity of the alpha synuclein fiber significantly decreased after Hsp27 adhered to the surface of alpha synuclein fiber.[42]

1.5 PROJECT GOAL AND HYPOTHESIS

Since the first discovery of Hsp27, the diverse pathological function of Hsp27 has been extensively investigated. The missing high-resolution atomic structure of full length Hsp27 is still the key needed for us to interpret the Hsp27 mechanism of prevent aberrant protein aggregation and its relationship to numerous diseases involved in neurodegeneration. This research will provide new insight to understanding the molecular interaction between Hsp27 and neurodegenerative disease related substrates.

The working hypothesis of this project is that both alpha synuclein fiber and tau fiber are able to bind to the Hsp27 intrinsic disorder domain, which allow the cryo-EM 3D reconstruction of the entire Hsp27-fiber complex to reveal the detail structural information of full length human Hsp27.

Chapter 2: Molecular Cloning

2.1 BACKGROUND OF MOLECULAR CLONING

Molecular cloning is a versatile technique in molecular biology that involves the process of amplifying a target gene of interest and then inserting gene into a desired expression vector plasmid. This engineered expression plasmid is then transformed into a compatible host expression system, which allow the overexpression of the recombinant protein. [43] The entire routes among molecular cloning are composed of polymerase chain reaction (PCR), restriction enzyme digestion and ligation, transformation and antibiotic selection. In general, the molecular cloning begins with polymerase chain reaction (PCR), which is the process to amplify target of gene to billions of copies. PCR works by cycling though repeated steps of double strand DNA denaturation, complementary primer annealing and new DNA strand extension. These three steps are typically repeated 25 to 30 cycles to obtain considerable amount of target interest for the downstream experiment. [44] The foundations of PCR reaction is the utilization of a thermophilic DNA polymerase that can withstand the initial high temperature denaturation step. Furthermore, the specifically designed primers complementary to the DNA template will initiate the synthesis of new single DNA strand. Nucleotides, which serve as the building blocks for the newly synthesized DNA strand.

Site-directed mutagenesis is a potent technique that allows for the introduction of specific mutations into the target of DNA, which includes substitution, insertion, and deletion. This technique is frequently used to investigate the impact of disease related mutation on protein structure and function. In order to successfully conduct the site directed mutagenesis, specific designed primers containing the target mutation, and using these primers in PCR reaction to amplify the mutated DNA templet.

After the gene of interest has been amplified to the desired concentration, restriction enzyme digestion is the following procedure in the molecular cloning process. This technique involves utilizing restriction enzymes to cut both ends of target of gene to create overhangs which enable the digested gene inserted to the desired expression vector plasmid. Restriction enzymes is able to recognize and cut at specific sequences of the double strand DNA. Majority of the restriction enzymes can recognize four to eight base pairs and hydrolyze phosphodiester bond of DNA strand. [45] Restriction enzymes can digest the DNA to create two different ends. The majority restriction enzymes is able to perform asymmetrically cut to create a single overhang referred to sticky end. Another type of restriction enzymes symmetrically digests double strand DNA to generate blunt end.

The following step is ligation. This process is to seal the digested gene and vector plasmid through formation of phosphodiester bond with conventional DNA ligase. [46] DNA ligases are indispensable enzymes which are found in all the species to modulate DNA replication. [47] DNA ligase can link the Okazaki fragments to create a continuous DNA strand. [48] With the supplement of ATP, the target of gene is covalently connected to the plasmid vector via DNA ligase to form a new construct. The gene is inserted in the 5' to 3' direction to ensure the successful transcription initiated by mRNA.

The expression vector, containing the target gene of interest, is then transformed into the desired expression host cell such as bacteria, yeast, or mammalian cell for recombinant protein production. Bacteria expression system has been considered as an excellent recombinant protein expression host due to several advantages. First, it has a fast growth rate, with cells reaching exponential growth phase a few hours after inoculation. Furthermore, the affordable media and high yield make bacterial cell an ideal candidate for recombinant protein expression. [49] In

order to introduce the vector plasmid into the expression cells, it is necessary to induce cells to uptake foreign DNA effectively.[50] Utilize calcium chloride or rubidium chloride to treat the expression cell is conventional chemical treatment, which has decent transformation efficiency. Calcium ion or rubidium ion can neutralize the negatively charged layer on surface of the expression cell membrane, allowing the exogenous plasmid vector to diffuse closely to the cell membrane and enter the expression cells more proficiently during the heat shock condition. [51,52] After transformation, it is necessary to verify the success of the process by performing an antibiotic selection. The majority of the expression plasmid contains the antibiotic resistance gene which encodes certain compounds to protect expression cell survive from growth media supplied with antibiotic. The expression cells containing the plasmid is able to grow on the selection LB plate containing the appropriate antibiotic. The overnight grown colonies can be inoculated to the liquid media and stored in -80°C with the addition of 25% glycerol to protect cell integrity for long term storage.

2.2 MATERIAL AND METHOD

The human α -synuclein gene, encoded by the SNAC gene was cloned into the expression vector pet-22b (+) using NdeI and XhoI restriction sites. Before the transformation, the concentration of the plasmid vector was determined using UV-VIS spectrometer to measure the absorbance at 260nm. 50 μ L of One Shot™ TOP10 Chemically Competent cell was thawed out on ice for 5 minutes. 4 μ L of the plasmid was added to the TOP10 cells and mixed by flicking 4 times. The plasmid was incubated with the competent cell on ice for 30 minutes. The cells were then heat shock by water bath at 42 °C for 10s. The competent cell was then incubated in the ice for 10 minutes. 1mL S.O.C. media were added to the cells in level two biosafety cabinet. The cells were recovered in incubator at 37°C for 1 hour with constant agitation at 220rpm. After recovered 1 hour, the transformed competent cells were inoculated on LB agar growth plate with 100 μ g/ μ L ampicillin. The LB plate was incubated for 16 hours at 37°C. The overnight grown colony was inoculated into 35mL 2XTY media containing 100 μ g/ μ L ampicillin. The cells were grown for 14 hours at 37°C with agitation at 220 rpm.

20mL of the overnight grown culture was centrifuged at 4000xg for 10 minutes. The supernatant was discarded, and the precipitated cell pellet was saved for plasmid purification with PureLink HiPure Plasmid Midiprep. The cell pellet was resuspended in 5mL of resuspending buffer. Then the cells were lysed using 5mL lysis buffer. After a brief incubation at room temperature, the cells were treated with 5mL precipitation buffer, and the tubes were gently inverted to make sure thoroughly mixed. The resulting cell lysate was centrifuged at 12,000xg for 30 minutes. A disposable Midi purification column was preequilibrated with 10mL of equilibration buffer. After 30 minutes centrifugation, the supernatant containing the target plasmid was transferred to the purification column and filtered by gravity. 10mL of washing

buffer was added to the column twice to clean the column membrane. Once all the washing buffer was eluted out from the column, the 4mL of prewarmed elution buffer was added to the column to elute out the plasmid vector. The elution was then treated with 3.5 mL of isopropanol to precipitate the plasmid. After centrifugation at 12,000xg for 30 minutes, the supernatant was discarded, and the precipitated plasmid was washed with 10mL of 70% ethanol. The cleaned plasmid vector was centrifuged at 12000xg for 10 minutes. The supernatant was discarded, and the plasmid vector was dried in the room temperature. The plasmid pellet was resuspended in 200 μ L Tri-base-EDTA (TE) buffer and the concentration was measured by the UV-vis spectrometer at 260nm wavelength.

The presence of target α -synuclein gene was quickly verified through polymerase chain reaction (PCR) before transformation to the BL21 cell. The target gene was amplified with commercially available Q5[®] DNA Polymerase (NEBiolabs) with the optimized setting. All the PCR reactions were executed with T7 promoter primer and T7 terminator primer ordered from Integrated DNA Technologies (IDT) 1nmol of purified plasmid with 0.5 μ M T7 promoter primer and T7 terminator primer were applied for the PCR reaction. The initial denaturation was performed for 30 seconds at 98 $^{\circ}$ C. Then annealing condition was set up at 69 $^{\circ}$ C for 30 seconds and followed by extension at 72 $^{\circ}$ C for 35 seconds. The target gene was amplified by 30 thermocycles. The end PCR product was verified by running 0.7% agarose gel supplied with SYBR Safe dye. The gel was checked using conventional blue light image machine.

50 μ L of BL21(DE3) expression cells were used for each plasmid vector transformation. The BL21 cells were thawed out on the ice for 5 minutes. 5ng of each plasmid vector were incubated with BL21 cell on the ice for 30 minutes. The competent cells were heat shocked for

30 seconds via water bath at 42°C. 500 µL of S.O.C media were added to each tube in biosafety cabinet. The competent cells were incubated at 37 °C with constant agitation at 220 rpm. After 1 hour, the BL21 competent cells were inoculated on the LB agar plate containing 100 µg/µL ampicillin. The LB agar plate was incubated at 37°C overnight to ensure colonies grown. The next day, three healthy grown colonies were inoculated in 2XTY media and verified the protein expression. The BL21 cell were grown in 2xTY media containing 100 µg/µL ampicillin until reach optical density (OD_{600}) at 0.6. 1 mM Isopropyl β- d-1-thiogalactopyranoside (IPTG) was added to the cell culture which induced for another 3 hours. 1 mL uninduced and induced sample was centrifuged down at 6000xg for 5 minutes. The precipitated cell pellet was resuspended in 400 µL of Milli-Q water. 5 µL of resuspended cell samples were mixed with 5 µL of 1X Lammeli SDS Buffer and denatured at 98°C for 5 minutes. The denatured samples were loaded at 10% sodium dodecyl sulfate–polyacrylamide gel (SDS-PAGE). The SDS-PAGE gels were performed at 210V for 40 minutes. After 40 minutes, the SDS-PAGE gels were stained with Commassie blue solution for 30 minutes followed by 30 minutes detaining. The colony with the normal expression of target proteins were grown in 35mL 2XTY media until OD_{600} reached 0.4. The 30mL of cell culture were mixed with 30mL autoclaved 50% glycerol solution to reach 25% glycerol as final working concentration. The glycerol stock was prepared in 1mL for each tube which flash frozen in liquid N₂ and stored in -80°C refrigerator.

2.3 RESULT

Figure 1 demonstrates the amplification of the SNCA gene and MAPT gene shown in solid bright bands at around 600 bp and 2000bp respectively.

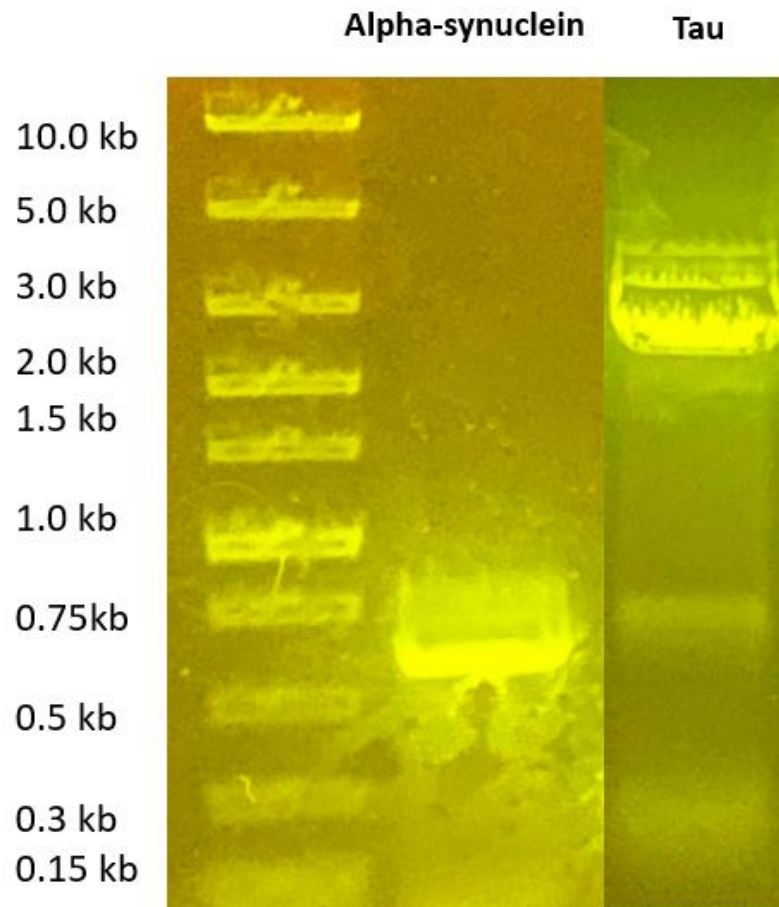


Figure2.1. 0.7% agarose gel of the PCR amplification end products. Alpha synuclein gene (SNCA) presents as solid bright band between 750 bp and 500bp in the second line. Tau gene (MAPT) presents as bright band slightly above 2000bp and one faint band around 750bp in third line.

2.4 DISCUSSION

The DNA agarose gel demonstrated that the PCR amplification products were shown very close to the expected position, indicating that their size was consistent with the theoretical size. The MAPT gene that encodes for Tau is 2277bp, and the bright band observed on the third line on the agarose gel was slightly above the 2000 bp DNA marker. The very faint band shown around the 750 bp could be due to the nonspecific binding of the T7 primers. T7 promoter and terminator primers are commonly utilized to quickly verify the presence of the target gene in the desired T7 promoter modulated plasmid vector. In general, T7 primers were designed to be complementary to the T7 promoter and terminator of the plasmid, with the target gene cloned in the multiple cloning site which is located between the T7 promoter and T7 terminator. Unlike the specific designed primer which is complementary to both ends of the target gene, the PCR amplification with T7 primers sometimes will cause nonspecific binding, which could explain the faint band observed on the DNA agarose gel. However, the band that appears around 2000bp was more dominant compared with the faint band. Thus, the presence of the MAPT gene in the pET-22b plasmid was successfully verified after Midi plasmid purification.

Chapter 3: Recombinant Protein Expression

3.1 BACKGROUND OF RECOMBINANT PROTEIN EXPRESSION

Recombinant protein expression refers to the process the target of proteins is synthesized and modified in desired expression organism, which is considered a critical step for various biochemistry researches. Through conventional molecular cloning techniques, the gene of interest is inserted into the desired expression vector which is transformed into the biocompatible expression organism. Via inducing the transcription of gene, the host organism is able to mass produce the recombinant protein. BL21 (DE3) is the most frequently used bacterial expression cell line for production of soluble cytosolic proteins. [53] The protein expression is controlled by the lac operon on the plasmid vector which is located before the target of gene. The lac operon is composed of three genes lacZ, Lac Y and Lac A, which encodes the essential housekeeping protein to regulate the E. coli metabolism.[54] The lac operon suppresser is located on the lac operon to inhibit the expression of the T7 RNA polymerase. With the addition of the IPTG which is a non-hydrolysable lactose analog, the lac operon suppresser is able to be removed, which allows the production of T7 RNA polymerase. The nascent synthesized T7 RNA polymerase can recognize the T7 promoter on the plasmid vector and subsequently initiate the transcription of the inserted target gene which is located downstream of the T7 promoter on the expression plasmid.[55]

In order to produce a substantial amount of recombinant target protein, sufficient amount of IPTG need to be added to induce the structural conformational change of lac operon suppresser, leading to its removal from the lac operon. Theoretically, the addition of lactose can also be applied to remove of the lac operon suppresser, which can activate the transcription of the target gene. While LacZ gene normally encodes beta-galactosidase that hydrolyzes lactose

into glucose and galactose, which will cause the significantly decrease the lactose availability. Eventually, the lac operon repressor will bind and inhibit the protein synthesis again.[56] Therefore, IPTG is substituted for the lactose to elevate the recombinant protein synthesis efficiency.

In order to effectively obtain target proteins from expression cell, cell lysis is the conventional approach to disrupt the cell membrane to effectively extract the cellular material from expression system. Cell lysis can be depicted in two classes which are mechanical method or non-mechanical method. For mechanical lysis approach, cell membrane is vigorously disrupted by physical force which can be generated from numerous techniques.[57] One of the popular mechanical lysis techniques is ultra-sonication which agitate the tissue or cells via high frequency sound wave. While one of the drawbacks of sonication is not compatible with relative fragile protein. The potent ultrasonication wave not only can agitate the outer cellular membrane but also can disrupt the intermolecular interaction of the protein, which causes the denaturation of the target protein. Alternatively, the addition of chemical or biological agents to lyse the bacterial cell can be employed. Lysozyme is frequently applied to hydrolyze the bacterial cell wall resulting to release the target proteins. Cell walls peptidoglycan can be effectively digested by the lysozyme which causes minimal detrimental effect of the protein to preserve protein in near native biological conformation.[58] Lysozyme can catalyze the cleavage of β (1-4) linkages between N-Acetylglucosamine and N-Acetylmuramic acid. The high-resolution crystal structure of lysozyme also reveals the fundamental mechanism of lysozyme catalytic process. [59] Lysozyme treatment is usually combined with another mild physical lysis method freeze and thaw cycles to elevate the lysis efficiency. The freezing process causes the generation of ice crystals on the cell membrane to facilitate disrupt the cell membrane. This method has been

demonstrated to be capable of releasing overexpressed recombinant proteins from expression cells but not releasing unwanted giant cytoplasmic E. coli protein. [60] However, freeze and thaw might be not compatible for temperature sensitive protein complex. Furthermore, time consuming is another disadvantage of this approach. Thus, the suitable lysis method needs to be considered based on the property of target protein.

After cell lysis, a significant amount of cellular material including DNA, RNA and numerous proteins are released from the E. coli cell. In order to prepare the lysate for downstream purification, all the nucleotides must be excluded from the protein mixture. The traditional approach is the addition of trace amount of deoxyribonuclease I (DNase) to effectively digest the bulk DNA into smaller fragments. DNase is a versatile endonuclease that can hydrolyze the phosphodiester linkage of one strand of nucleotide. This enzyme is able to recognize the cleavage site between 3' oxygen atom and the neighbor phosphorus atom.[60] The presence of magnesium ion is critical cofactor for maintaining its enzymatic activity. Following the DNase treatment, 3% of streptomycin sulfate is added to the lysate to effectively separate digested small nucleotide fragment from protein mixture.[61] After the high-speed centrifugation at low temperature, cellular debris and unwanted DNA material will precipitate from the lysate and the soluble protein mixture will remain in the top supernatant for future purification.

3.2 MATERIAL AND METHOD

Alpha synuclein cell cultures were inoculated from 1mL flash frozen 25% glycerol stock. 1mL glycerol stock was added to the 1L of 2XTY media supplied with 100 mg/mL ampicillin. The cell culture was grown in 2.5 L culture flask at 37 °C with constant agitation. The cell culture grew until cell density OD₆₀₀ reached 0.6. Then 1mL 1M IPTG stock was added to the culture to reach final working concentration of 1 mM. The cells were induced for another 3 hours at 37 °C. Cells were harvested through centrifugation at 6000xg for 20 minutes. The collected cell pellet was resuspended in lysis buffer (25mM Tris-base, 50mM NaCl, 5mM EDTA). The cell pellet was resuspended in 1 to 3 ratio. Lysozyme stock was added to the cell lysate to reach the final work concentration of 0.2 mg/mL. The lysozyme treatment was performed for 45 minutes at 4 °C on the HulaMixer. The lysate was completely frozen in -20 °C refrigerator and thawed out at the room temperature. The freeze and thaw cycle were executed 3 times. After the third thaw out, 1 M MgCl₂ stock was added to the cell lysate to reach 100 mM final concentration. DNase stock was added to the 0.1 mg/mL. The DNase digestion was performed for 1 hour at 4 °C on the HulaMixer. The streptomycin sulfate was added to 3% (w/v) and lysate was incubated until becoming less viscous. Cell lysate was centrifuged at 12,000xg for 30 minutes. The precipitate pellet was discarded, and supernatant was added with a room temperature saturated ammonium sulfate stock solution to reach final concentration of 30%. The lysate was then incubated at HulaMixer for another 30 minutes at 4 °C. After 30 minutes, the lysate was centrifuged at 12,000xg for 30 minutes and the precipitated protein pellet was discarded. The room temperature ammonia sulfate stock solution was added to the collected supernatant to reach final concentration of 40%. The cell lysate was incubated again for another 30 minutes at 4 °C and then centrifuged at 12,000xg for 30 minutes. The supernatant was

discarded, and the protein pellet was resuspended in 3 mL ion exchange buffer A (20mM Tris-base, 5mM EDTA pH= 7.5). The resuspended protein was aliquoted into the 1.5 mL high centrifuge speed Eppendorf tube and flash freeze in liquid nitrogen stored in -80 °C refrigerator for long term storage.

Tau cell cultures were inoculated from 1mL flash frozen 25% glycerol stock. 1mL glycerol stock was added to the 1L of 2XTY media supplied with 100 mg/mL ampicillin. The cell culture was grown in 2.5 L culture flask at 37 °C with constant agitation. The cell culture was grown until cell density OD₆₀₀ reached 0.8. Then 1mL 1M IPTG stock was added to the culture to reach final working concentration of 0.5 mM. The cells were induced for another 4 hours at 30 °C. Cells were harvested through centrifugation at 6000xg for 20 minutes. The collected cell pellet was resuspended in lysis buffer (20mM Tris-base, 100mM NaCl, 5mM EDTA). The cell pellet was resuspended in 1 to 4 ratio. Lysozyme stock was added to the cell lysate to reach the final work concentration 0.25 mg/mL. The lysozyme treatment was performed for 60 minutes at 4 °C on the HulaMixer. The lysate was completely frozen in -20 °C refrigerator and thaw out at the room temperature. The freeze and thaw cycle were executed 2 times. After the second thaw out, 1 M MgCl₂ stock were added to the cell lysate to reach 100 mM final concentration. DNase stock was added to the 0.15 mg/mL. The DNase digestion was performed for 1 hour at 4 °C on the HulaMixer. The streptomycin sulfate was added to 3% (w/v) and lysate was incubated for an additional 60 minutes. Cell lysate was centrifuged at 12,000xg for 30 minutes. The precipitate pellet was discarded, and supernatant was added with a room temperature saturated ammonium sulfate stock solution to reach final concentration of 25%. The lysate was then incubated at HulaMixer for another 30 minutes at 4 °C. After 30 minutes, the lysate was centrifuged at 12,000xg for 30 minutes and the precipitated protein pellet was

discarded. The room temperature ammonia sulfate stock solution was added to the collected supernatant to reach final concentration of 35%. The cell lysate was incubated again for another 30 minutes at 4 °C and then centrifuged at 12,000xg for 30 minutes. The supernatant was discarded, and the protein pellet was resuspended in 6 mL ion exchange buffer A (20mM Tris-base, 50mM NaCl, 1mM EDTA pH= 6.9). The resuspended protein was aliquoted into the 1.5 mL high centrifuge speed Eppendorf tube and flash freeze in liquid nitrogen stored in -80 °C refrigerator for long term storage.

Hsp27 wild type cell cultures were inoculated from 1mL flash frozen 25% glycerol stock. 1mL glycerol stock was added to the 1L of 2XTY media supplied with 100 mg/mL ampicillin. The cell culture was grown in 2.5 L culture flask at 37 °C with constant agitation. The cell culture was grown until cell density OD_{600} reach 0.6. Then 1mL 1M IPTG stock was added to the culture to reach final working concentration of 0.05 mM. The cells were induced for another 18 hours at 15°C. Cells were harvested through centrifugation at 6000xg for 20 minutes. The collected cell pellet was resuspended in lysis buffer (25mM HEPES, 100mM NaCl, 20mM EDTA, pH=7.5). The cell pellet was resuspended in 1 to 3 ratio. Lysozyme stock was added to the cell lysate to reach the final work concentration of 0.2 mg/mL. The lysozyme treatment was performed for 45 minutes at 4 °C on the HulaMixer. The lysate was completely frozen in -20 °C refrigerator and thawed out at room temperature. The freeze and thaw cycle were executed 3 times. After the third thaw out, 1 M $MgCl_2$ stock was added to the cell lysate to reach 60 mM final concentration. DNase stock was added to the 0.1 mg/mL. The DNase digestion was performed for 1 hour at 4 °C on the HulaMixer. The streptomycin sulfate was added to 3% (w/v) and lysate was incubated until becoming less viscous. Cell lysate was centrifuged at 12,000xg for

30 minutes. The precipitate pellet was discarded, and supernatant was added with a room temperature saturated ammonium sulfate stock solution to reach final concentration of 25%. The lysate was then incubated at HulaMixer for another 30 minutes at 4 °C. After 30 minutes, the lysate was centrifuged at 12,000xg for 30 minutes and the precipitated protein pellet was discarded. The room temperature ammonia sulfate stock solution was added to the collected supernatant to reach final concentration of 35%. The cell lysate was incubated again for another 30 minutes at 4 °C and then centrifuged at 12,000xg for 30 minutes. The supernatant was discarded, and the protein pellet was resuspended in 3 mL ion exchange buffer A (20mM HEPES, 5mM EDTA pH= 7.5). The resuspended protein was aliquoted into the 1.5 mL high centrifuge speed Eppendorf tube and flash freeze in liquid nitrogen stored in -80 °C refrigerator for long term storage.

Human MAP kinase-activated protein kinase 2 (MAPKAPK2) constitutively active triple serine mutants cell cultures were inoculated from 1mL flash frozen 25% glycerol stock. 1mL glycerol stock was added to the 1L of 2XTY media supplied with 100 mg/mL kanamycin. The cell culture was grown in 2.5 L culture flask at 37 °C with constant agitation. The cell culture was grown until cell density OD₆₀₀ reach 0.6. Then 1mL 1M IPTG stock was added to the culture to reach final working concentration of 0.2 mM. The cells were induced for another 3 hours at 30°C. Cells were harvested through centrifugation at 6000xg for 20 minutes. The collected cell pellet was resuspended in lysis buffer (25mM HEPES, 100mM NaCl, 20mM EDTA, pH=7.5). The cell pellet was resuspended in 1 to 3 ratio. Lysozyme stock was added to the cell lysate to reach the final work concentration of 0.2 mg/mL. The lysozyme treatment was performed for 45 minutes at 4 °C on the HulaMixer. The lysate was completely frozen in -20 °C

refrigerator and thaw out at the room temperature. The freeze and thaw cycle were executed 3 times. After the third thaw out, 1 M MgCl₂ stock was added to the cell lysate to reach 60 mM final concentration. DNase stock was added to the 0.1 mg/mL. The DNase digestion was performed for 1 hour at 4 °C on the HulaMixer. The streptomycin sulfate was added to 3% (w/v) and lysate was incubated until becoming less viscous. Cell lysate was centrifuged at 12,000xg for 30 minutes. The precipitate pellet was discarded, and supernatant was added with a room temperature saturated ammonium sulfate stock solution to reach final concentration of 30%. The lysate was then incubated at HulaMixer for another 30 minutes at 4 °C. After 30 minutes, the lysate was centrifuged at 12,000xg for 30 minutes and the precipitated protein pellet was discarded. The room temperature ammonia sulfate stock solution was added to the collected supernatant to reach final concentration of 50%. The cell lysate was incubated again for another 30 minutes at 4 °C and then centrifuged at 12,000xg for 30 minutes. The supernatant was discarded, and the protein pellet was resuspended in 4 mL ion exchange buffer A (20mM HEPES, 5mM EDTA pH= 6.7). The resuspended protein was aliquoted into the 1.5 mL high centrifuge speed Eppendorf tube and flash freeze in liquid nitrogen stored in -80 °C refrigerator for long term storage.

Human Hsp27 constitutively active triple serine mutants cell cultures were inoculated from 1mL flash frozen 25% glycerol stock. 1mL glycerol stock was added to the 1L of 2XTY media supplied with 100 mg/mL ampicillin. The cell culture was grown in 2.5 L culture flask at 37 °C with constant agitation. The cell culture was grown until cell density OD₆₀₀ reach 0.6. Then 1mL 1M IPTG stock was added to the culture to reach final working concentration of 0.05 mM. The cells were induced for another 20 hours at 15 °C. Cells were harvested through centrifugation at 6000xg for 20 minutes. The collected cell pellet was resuspended in lysis buffer

(20mM HEPES, 100mM NaCl, 20mM EDTA, pH=7.5). The cell pellet was resuspended in 1 to 3 ratio. Lysozyme stock was added to the cell lysate to reach the final work concentration 0.25 mg/mL. The lysozyme treatment was performed for 60 minutes at 4 °C on the HulaMixer. The lysate was completely frozen in -20 °C refrigerator and thaw out at the room temperature. The freeze and thaw cycle were executed 2 times. After the second thaw out, 1 M MgCl₂ stock was added to the cell lysate to reach 100 mM final concentration. DNase stock was added to the 0.1 mg/mL. The DNase digestion was performed for 1 hour at 4 °C on the HulaMixer. The streptomycin sulfate was added to 3% (w/v) and lysate was incubated for an additional 60 minutes. Cell lysate was centrifuged at 12,000xg for 30 minutes. The precipitate pellet was discarded, and supernatant was added with a room temperature saturated ammonium sulfate stock solution to reach final concentration of 25%. The lysate was then incubated at HulaMixer for another 30 minutes at 4 °C. After 30 minutes, the lysate was centrifuged at 12,000xg for 30 minutes and the precipitated protein pellet was discarded. The room temperature ammonia sulfate stock solution was added to the collected supernatant to reach final concentration of 40%. The cell lysate was incubated again for another 30 minutes at 4 °C and then centrifuged at 12,000xg for 30 minutes. The supernatant was discarded, and the protein pellet was resuspended in 4 mL ion exchange buffer A (20mM HEPES, 100mM NaCl, 5mM EDTA pH= 7.5). The resuspended protein was aliquoted into the 1.5 mL high centrifuge speed Eppendorf tube and flash freeze in liquid nitrogen stored in -80 °C refrigerator for long term storage.

3.3 RESULT

Figure 3.1 depicted the results of the SDS-PAGE analysis conducted to assess the expression condition of alpha synuclein. The first line in the figure represented the protein marker, while the second line corresponded to the uninduced cell culture sample. The third and fourth lines illustrated the induced cell culture samples. Following a 3-hour induction period, a substantial amount of recombinant alpha synuclein was successfully obtained. Notably, no leaky expression was observed in the uninduced sample, indicating a tightly regulated expression. These findings suggested that the induced expression condition of alpha synuclein may be an effective means of producing the protein for further research purposes.

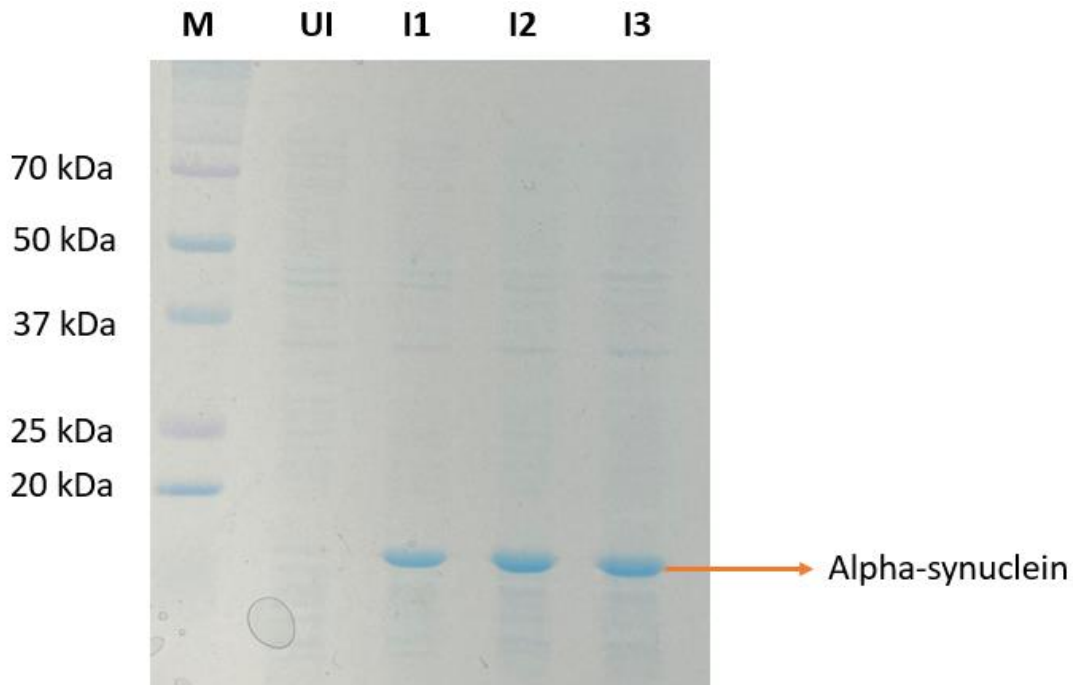


Figure 3.1: 10% SDS-PAGE of the human alpha synuclein protein expression conditions. Line 1 protein marker, line 2 uninduced cell sample, line 3 to 5 induced cell sample with solid sharp band around 14.4 kDa.

Figure 3.2 displays the SDS-PAGE results obtained from evaluating the expression conditions of human Tau protein. As expected, the protein was detected at the anticipated position of approximately 110 kDa. However, the expression level of Tau was significantly lower in comparison to that of alpha synuclein. Although the expression level of Tau was lower, these results provide valuable insight into the protein's expression conditions, which could be useful for optimizing its production in future studies. Further investigation may be necessary to identify factors that could impact Tau expression.

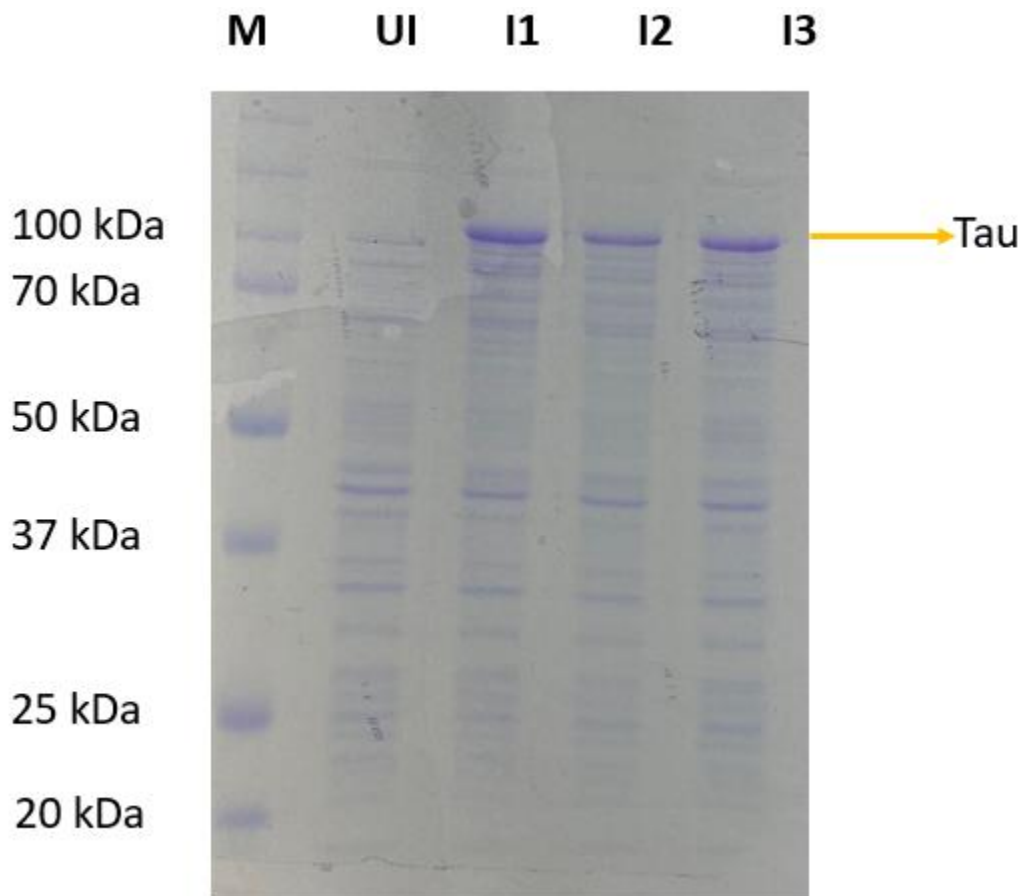


Figure 3.2: 7.5% SDS-PAGE of the human Tau protein expression conditions. Line 1 protein marker, line 2 uninduced cell sample, line 3 to 5 induced cell sample with solid sharp band around 110 kDa

Figure 3.3 depicts the SDS-PAGE result obtained from analyzing the expression level of wild type human heat shock protein 27 (Hsp27). Notably, the expression level of Hsp27 was found to be high. These findings suggest that the expression system applied in this study was effective in producing significant quantities of Hsp27.

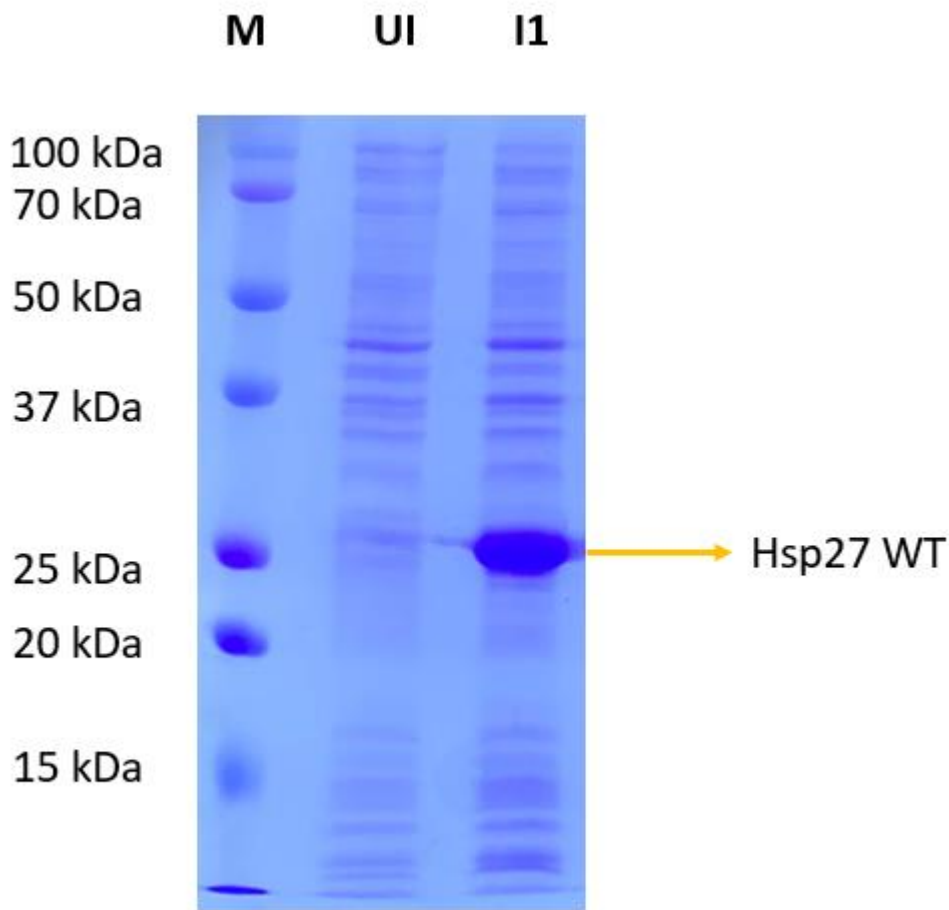


Figure 3.3: 12.5% SDS-PAGE of the human Hsp27 WT protein expression conditions. Line 1 protein marker, line 2 uninduced cell sample, line 3 induced cell sample with solid sharp band around 27 kDa.

The SDS-PAGE result obtained from evaluating the expression of constitutively active serine mutants of human heat shock protein 27 (Hsp27) was presented in Figure 3.4. Notably, the expression level of the mutants was almost identical to that of the wild type Hsp27. However, in the second line of the figure representing the uninduced sample, leaky expression was observed.

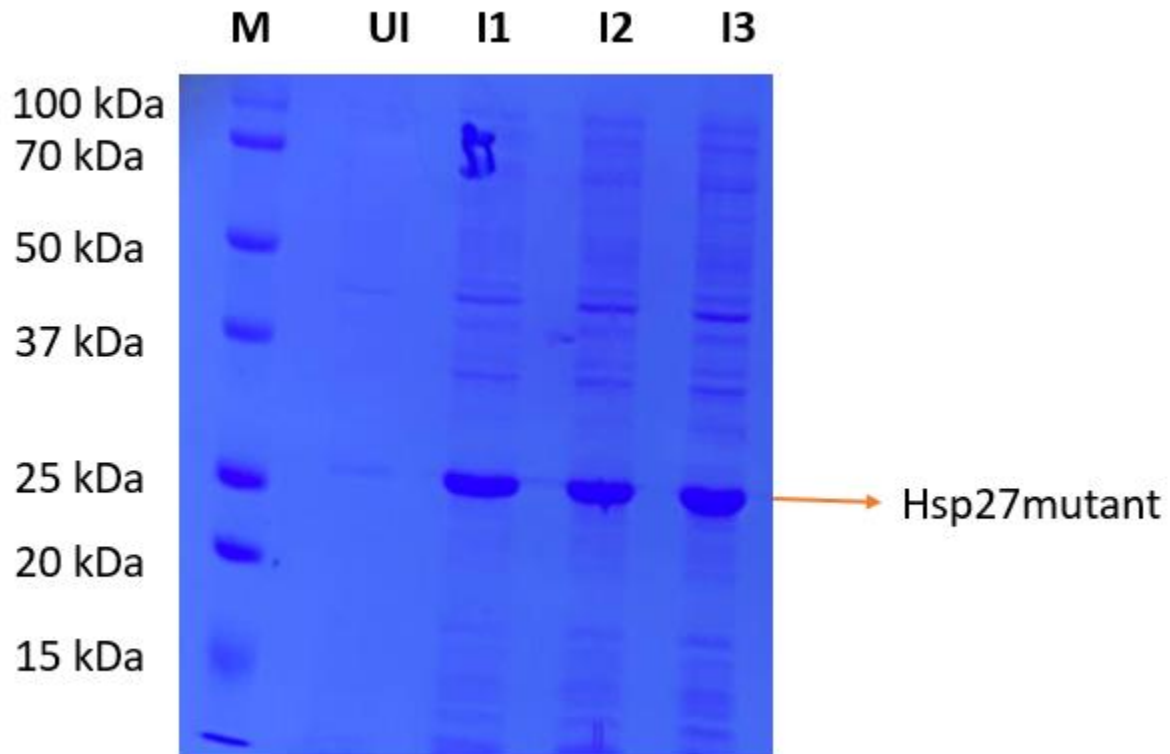


Figure 3.4: 12.5% SDS-PAGE of the human heat shock protein 27 constitutively active serine mutant protein expression conditions. Line 1 protein marker, line 2 uninduced cell sample, line 3 to 5 induced cell sample with solid sharp band around 27 kDa

The results of the SDS-PAGE analysis conducted on Tau ammonium sulfate precipitation was presented in Figure 3.5. To prepare the protein mixture, cell debris was separated from the lysate and subsequently treated with room temperature ammonium sulfate solution, increasing the final concentration from 30% to 45% saturation in 5% increments with each addition. Following each round of ammonium sulfate precipitation, the resulting protein pellet and remaining supernatant was resuspended in water, mixed with SDS sample buffer, and analyzed on a 7.5% SDS-PAGE gel.

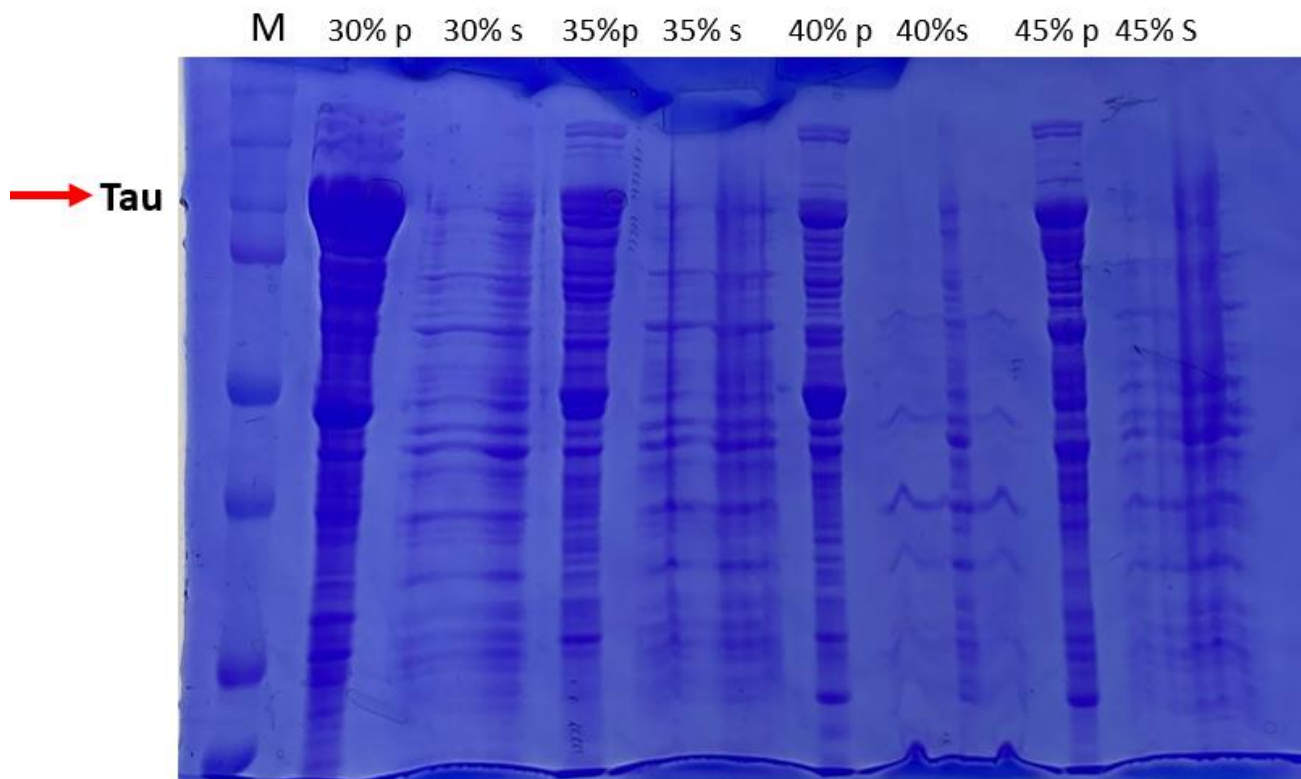


Figure 3.5. 7.5% SDS-PAGE of the Tau ammonium sulfate precipitate optimization. Line 1: protein marker. Line 2 resuspended protein pellet at 30% ammonium sulfate. Line 3: supernatant at 30% ammonium sulfate saturation. Line 4: resuspended protein pellet at 35% ammonium sulfate. Line 4: supernatant at 35% ammonium sulfate saturation. Line 5: supernatant at 35% ammonium sulfate saturation. Line 6: resuspended protein pellet at 40% ammonium sulfate precipitation. Line 6: supernatant at 40% ammonium sulfate saturation. Line 7: resuspended protein pellet at 45% ammonium sulfate precipitation. Line 8: supernatant at 45% ammonium sulfate saturation.

SDS-PAGE result of alpha synuclein ammonium sulfate precipitation was shown in Figure 3.6. After separation of cell debris from lysate, the protein mixture was subsequently treated with room temperature ammonium sulfate solution to reach final concentration from 25% to 60% saturation with 5% increment for each addition. Each round ammonium sulfate precipitated protein pellet was resuspended with water and mixed with SDS sample buffer and verified on the 12.5% SDS-PAGE.

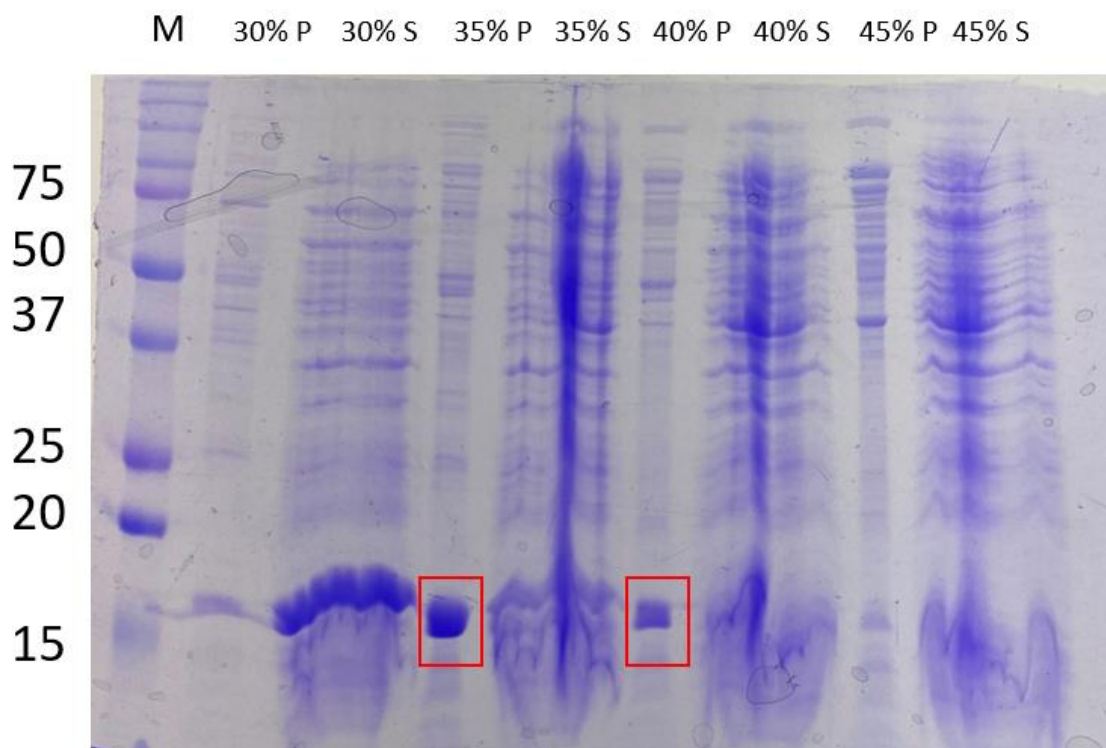


Figure 3.6. 12.5% SDS-PAGE of the alpha synuclein ammonium sulfate precipitate optimization. Line 1: protein marker. Line 2 resuspended protein pellet at 30% ammonium sulfate. Line 3: supernatant at 30% ammonium sulfate saturation. Line 4: resuspended protein pellet at 35% ammonium sulfate. Line 4: supernatant at 35% ammonium sulfate saturation. Line 5: supernatant at 35% ammonium sulfate saturation. Line 6: resuspended protein pellet at 40% ammonium sulfate precipitation. Line 6: supernatant at 40% ammonium sulfate saturation. Line 7: resuspended protein pellet at 45% ammonium sulfate precipitation. Line 8: supernatant at 45% ammonium sulfate saturation.

3.4 DISCUSSION

Based on the SDS-PAGE results, a substantial amount of alpha synuclein was able to be obtained from 3-hour induction at 37 °C. While the expression level of the Tau was significantly lower compared with alpha synuclein. Based on the preliminary expression optimization of Tau, induction at 30°C for 3 hours resulted in the highest expression level. There were no leaky expression issues occurred for both alpha synuclein and Tau. Notably, the expression level of Hsp27 WT is the highest among all the proteins. In comparison to induce at 30°C or 37°C, low temperature overnight induction significantly enhanced the Hsp27 WT solubility and maintained a high protein expression level. Interestingly, the expression condition of Hsp27 constitutively active serine mutant was very similar to those of the Hsp27. However, in contrast to the Hsp27 WT, a faint band around 27 kDa was observed in the second line on the SDS-PAGE of uninduced samples of the Hsp27 constitutively active serine mutant, indicating the occurrence of leaky expression. In comparison to the expression levels observed in the induced sample on line 3, the extent of leaky expression in uninduced samples was relatively negligible. Given that leaky expression is a common issue with the pET expression system, these findings suggest that additional optimization may not be necessary to completely inhibit this phenomenon.

The SDS-PAGE results obtained from the ammonium sulfate precipitation demonstrated that approximately 90% of Tau presented in the cell lysate was successfully precipitated at 30% ammonium sulfate saturation, as evidenced by the dominant band observed at around 110 kDa in line 2 of Figure 3.5. However, approximately 10% of the Tau remained in the supernatant even after precipitation at this saturation level. Based on the results of line 5, all the Tau was able to be collected through ammonium sulfate precipitation at 35% saturation. Similarly for alpha synuclein, the initial ammonium sulfate precipitation step at 35% saturation resulted in the

precipitation of about 80% of the protein, as indicated by the dominant band around 14.5 kDa in line 4 of Figure 3.6. However, there was still about 20% of the protein remaining in the cell lysate. To recover this residual protein, the cell lysate was subjected to another round of ammonium sulfate precipitation at 40% saturation, resulting in the band shown in line 6 of Figure 3.6.

Through exploiting *E. coli* expression system, all the targets protein successfully overexpressed and remain in soluble native conformation. After the initial ammonium sulfate precipitation, the proteins of interest were able concentrated from the protein mixture and briefly purified. The flash freeze resuspended ammonium sulfate precipitation protein pellet was ready for the downstream protein chromatograph purification.

Chapter 4: Protein Chromatography Purification

4.1 BACKGROUND OF PROTEIN CHROMATOGRAPHY

In order to perform the enzymatic or structural investigation of target protein, protein has to be purified from crude mixture to reach high purity to eliminate impact from undesired proteins. In recent years, Fast protein liquid chromatograph (FPLC) has emerged as the robust approach to extract protein of interest from the protein mixture in modern biochemistry research. This approach is able to reproducibly purify a variety of biomolecules with high resolution. The system can precisely load the protein mixture referred to as mobile phase to interact with the stationary phase which is the column composed of microscopic resin with the sample pump to separate the target protein from crude protein mixture.[62] Conventional chromatography used for protein purification includes ion exchange chromatography, size exclusion chromatography, affinity chromatography, and hydrophobic interaction chromatography. Each type of chromatography exploits a distinct property such as the net charge, hydrophobicity and overall size and shape of the target protein and can be used alone or in combination to achieve the desired purity. Once protein is loaded to the purification column, protein will either bind to the chromatograph column or pass through it. Under the designated condition, the target protein will elute out from the column resulting in a unique elution profile can be monitored by a highly sensitive UV detector. In general, there are several type of chromatographs which can be exploited for the protein purification. In order to reach high resolution and preserve protein native conformation, it is imperative to carefully select the appropriate type of and the purification condition has to be carefully optimized accordingly.

Ion exchange chromatography is broadly utilized approach for the initial purification of crude protein samples. This technique is particularly effective for separating proteins according

to the overall surface charge difference of protein. The ion exchange column is compatible with fast flow rate, routinely used salts, which make its idea for initial stage purification. The separation process is dictated by the degree of protein interaction to the compatible ion exchange column. [63] In order to achieve optimal separation resolution, numerous parameters have to be carefully considered such as buffer pH, ionic strength and type of resin for each target protein. [64] Ion exchange chromatography can be classified as two categories, the anion exchange chromatograph and cation exchange chromatography. The name indicates the charge of the column that target of biomolecular can bind to. The anion exchange column is packed with positive charged functional group which enable the overall negative charged protein to bind to it. The common positive charged functional group for strong anion exchange is quaternary ammonium, which enables superior separation in broad range of pH. On the other hand, the sulfonic acid or carboxymethyl negative charged functional group are frequently exploited for the cation exchange column. In order to perform the ion exchange chromatography, the overall net charge of target of protein under working pH must be determined. The isoelectric point (PI) is the critical property of target protein to dictate protein overall surface charge. This property is determined via the sum of dissociation constant values of the individual primary amino acid sequence. Based on preliminary research, the theoretical calculated PI based on the primary amino acid sequence matches with the experimental investigated value. Various computational programs have been applied to precisely estimating protein overall net charge for the downstream applications.[65]

Elution of bound proteins in ion exchange chromatograph is dependent on the salt concentration of buffer, specifically the overall ionic strength. Protein mixtures are prepared in the appropriate equilibration buffer with very low ionic strength and an ideal pH environment,

which allow charged protein binding to the column, while proteins with zero charged or same charged as resin protein will flow through the column. Then, the ion exchange column is washed with the equilibration buffer to remove nonspecifically bound proteins. The elution is conducted through increasing the amount of salt in the buffer, which disrupts the ionic interaction between bound protein to the resin. Since proteins have various levels of charge, the protein with lower charged will elute earlier. At a specific salt concentration, the target protein will elute out from the column and subjected for downstream experiments.

Size elution chromatograph (SEC) is complementary technique frequently used in conjunction with Ion exchange chromatograph to further purify the target of protein. Moreover, SEC has been utilized for aggregation assessment and protein size validation.[66] Size elution chromatograph is able to separate the protein based on their size and shape. Size elution chromatograph column is packed of microscopic agarose beads which have many porous on the surface. The smaller protein is able to enter the pores and travel through the entire column. While the larger globular protein will bypass the agarose bead resulting in earlier elusion. Thus, larger proteins are excluded and pass around the beads. As a result, proteins are eluted in order of decreasing size, with the smallest proteins eluting last. Additionally, SEC can be exploited to evaluate the size and oligomeric state of protein complexes, making it a potent technique in structural biology research. However, intrinsic disordered protein or elongated folded protein may have physical shape that are not proportional to their molecular weight, leading to earlier elution than expected. The entire separation is dictated on the size of the pores and to reach highest resolution, the effective separation range of the SEC column must be compatible to the size of the target protein.[67] In addition to its role in final polishing step, SEC is frequently

utilized for the buffer exchange process as well. SEC only requires one type of elution buffer that is dictated by the downstream experiment condition.

Hydrophobic interaction chromatography is another conventional technique which enables the analytical scale purification of the crude protein mixture. Unlike the ion exchange chromatography, hydrophobic interaction chromatography separates proteins according to the hydrophobicity differences. The hydrophobic column is packed with the resin which covalently links to various hydrophobic function ligands such as t-Butyl or other aromatic functional groups. The protein mixture is prepared in the high salt buffer, which enhances the binding to the resin. In general, the linear decreasing of salt concentration is applied to elute out the target protein. As the salt concentration decreases, the solvation of protein increases. The least hydrophobic protein will elute from the column earlier than the relative hydrophilic one. Due to the robust performance, the hydrophobic interaction chromatography can substitute the ion exchange chromatography as the initial purification. The elution then can be concentrated to small volume and further purified by the SEC. The high concentration salt can be exchanged to the desired buffer for the following process.

4.2 MATERIAL AND METHOD

Alpha synuclein was purified via dissolving 1mL of flash freeze ammonium sulfate prep in the 20 mL Ion exchange buffer A. The diluted protein mixture is loaded to the 5mL HiTrap Q column pre-equilibrated with Ion exchange buffer A. The column was washed with 25mL (5 column volumes) of buffer A. The elution was performed through step gradient. The first elution was set at step gradient of 18% ion exchange buffer B (20mM Tris, 1M NaCl, pH=7.5) for 6 column volumes. The second step was set at 22% of buffer B for an additional 6 column volumes. The fractions were collected at 25 mS/cm and concentrated to 1mL using an MilliporeSigma™ Amicon™ Ultra-15 Centrifugal Filter Units. The concentrated protein was diluted to the 10mL of hydrophobic buffer A and loaded to the pre-equilibrated 5mL HiTrap Butyl HP column (GE Healthcare). The elution was executed through an ammonium sulfate linear gradient from 1.5 M to 0 M over 20 column volumes. The fractions were collected at 150 mS/cm conductivity and concentrated to 500 μ l. The concentrated protein was loaded onto a Superose 6 Increase 10/300 GL (GE Healthcare) gel filtration column with 0.4 ml/minute flow rate. The fractions from 27 to 35 were collected and concentrated to 300uL. The purified protein concentration was evaluated through Pierce™ BCA Assay (Thermo Fisher Scientific). The fractions collected from each chromatograph was verified by running through the 10% SDS-PAGE gel at 210 V for 40 minutes.

Tau was purified via dissolving 2mL of flash freeze ammonium sulfate prep in the 75 mL Ion exchange buffer A. The diluted protein mixture is loaded to the 5mL HiTrap SP (GE Healthcare) column pre-equilibrated with Ion exchange buffer A. The column was washed with 25mL (3 column volumes) of buffer A. The elution was performed through step gradient. The first elution was set at step gradient of 18% ion exchange buffer B (20 mM Tris, 1 M NaCl, 1

mM EDTA, pH=6.9) for 6 column volumes. The second step was set at 22% of buffer B for an additional 6 column volumes. The fractions were collected at 25 mS/cm and concentrated to 500 μ L using an MilliporeSigma™ Amicon™ Ultra-15 Centrifugal Filter Units. The concentrated protein was loaded onto a Superose 6 Increase 10/300 GL (GE Healthcare) gel filtration column with 0.4 ml/minute flow rate. The fractions from 19 to 26 were collected and concentrated to 100 μ L. The purified protein concentration was evaluated through Pierce™ BCA Assay (Thermo Fisher Scientific). The fractions collected from each chromatograph was verified by running through 7.5% SDS-PAGE gel at 210 V for 40 minutes.

Human Hsp27 WT and Hsp27 constitutively active mutant were purified through identical approach. Hsp27 WT or mutant was purified via dissolving 1mL of flash freeze ammonium sulfate prep in the 20 mL Ion exchange buffer A. The diluted protein mixture is loaded to the double 5mL HiTrap Q column pre-equilibrated with Ion exchange buffer A. The column was washed with 25mL (5 column volumes) of buffer A. The elution was performed through linear gradient from 0 M to 1 M over 10 column volume. The fractions were collected at 20 mS/cm and concentrated to 500 μ L using an MilliporeSigma™ Amicon™ Ultra-15 Centrifugal Filter Units. The concentrated protein was loaded onto a Superose 6 Increase 10/300 GL (GE Healthcare) gel filtration column with 0.4 ml/minute flow rate. The fractions from 28 to 39 were collected and concentrated to 250 μ L. The purified protein concentration was evaluated through Pierce™ BCA Assay (Thermo Fisher Scientific). The fractions collected from each chromatograph was verified by running through the 12.5 % SDS-PAGE gel at 210 V for 40 minutes.

MAPKAPK2 was purified via dissolving 1mL of flash freeze ammonium sulfate prep in the 20 mL Ion exchange buffer A. The diluted protein mixture is loaded to the 5mL HiTrap SP

(GE Healthcare) column pre-equilibrated with Ion exchange buffer A. The column was loaded with 20mL (4 column volumes) of buffer A. The elution was performed through linear gradient from 0 M to 1M over 20 column volumes. The fractions were collected at 25 mS/cm and concentrated to 500 μ L using an MilliporeSigma™ Amicon™ Ultra-15 Centrifugal Filter Units. The concentrated protein was loaded onto a Superose 6 Increase 10/300 GL (GE Healthcare) gel filtration column with 0.4 ml/minute flow rate. The fractions from 19 to 26 were collected and concentrated to 200 μ L. The purified protein concentration was evaluated through Pierce™ BCA Assay (Thermo Fisher Scientific).

4.3 RESULT

Ion exchange chromatogram and SDS-PAGE analysis of alpha synuclein was employed to evaluate the purity of target protein. Alpha synuclein was observed at 14.5 kDa and was eluted out at second peak with 22% buffer B step gradient. The fraction from F32 to F42 was collected, mixed with SDS sample buffer, and analyzed using SDS-PAGE gel. The SDS-PAGE gel Figure 4.2 demonstrated the purity of alpha synuclein from Ion exchange column was proximately 80% purity, with the most dominant band around 14.5 kDa representing target protein. Several bands representing impurity proteins were also visible. The collected fractions were concentrated for the hydrophobic interaction chromatograph in order to reach over 95% purity for downstream experiments.

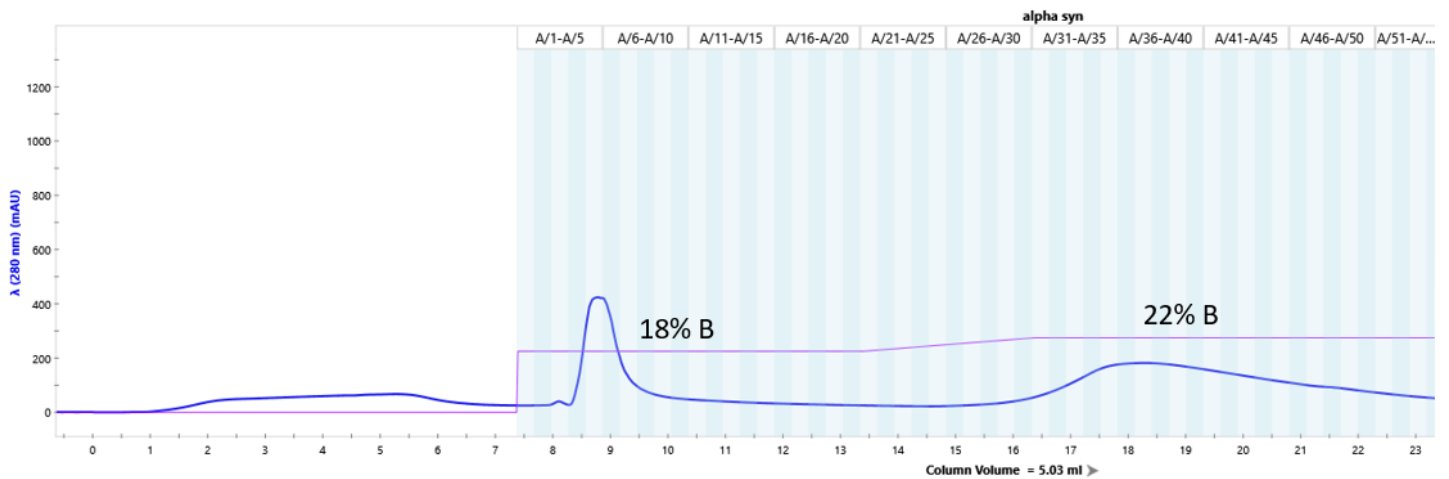


Figure 4.1 Ion exchange chromatography of alpha synuclein

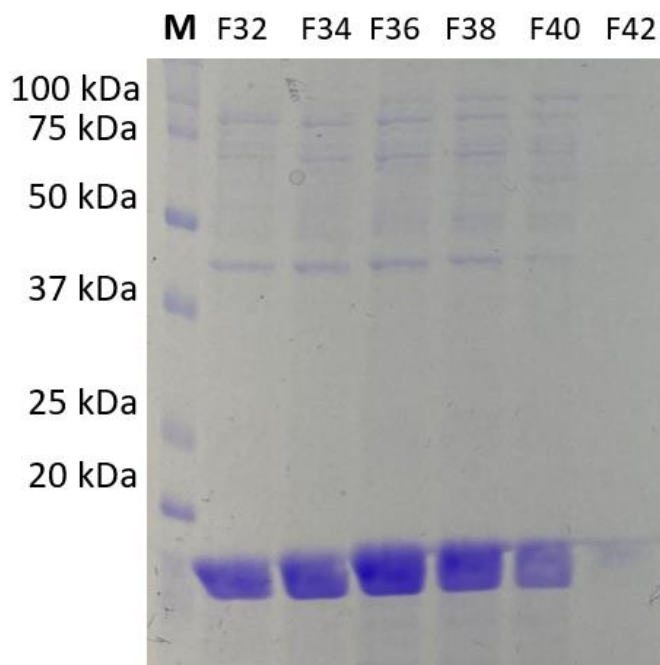


Figure 4.2 12.5 % SDS-PAGE of alpha synuclein fractions from Ion exchange column

Hydrophobic chromatogram revealed the elution profile of alpha synuclein, where a linear salt gradient was applied to elute the target protein. Fractions from F36 to F50, which eluted at 150 mS/cm conductivity, were found to contain the alpha synuclein. The SDS-PAGE gel Figure 4.4 demonstrated the alpha synuclein from hydrophobic column had a purity of proximately 93%.

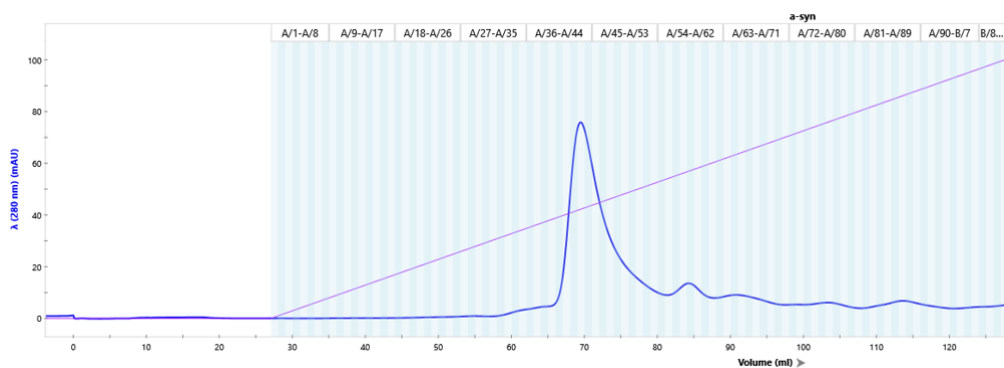


Figure 4.3 Hydrophobic interaction chromatography of alpha synuclein

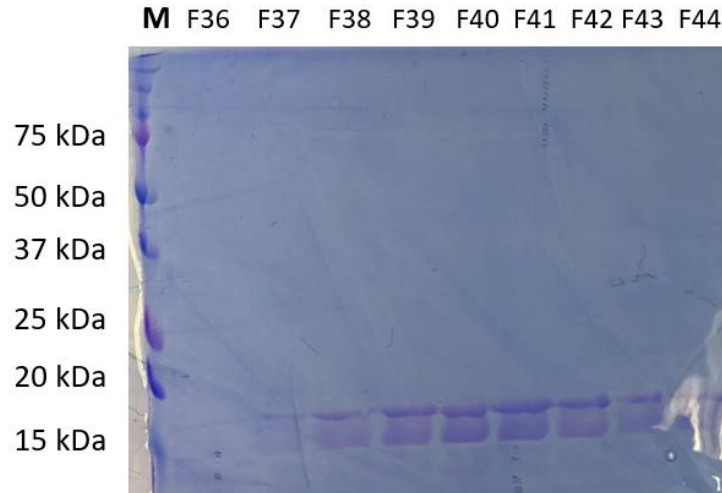


Figure 4.4 12.5% SDS-PAGE of fractions from hydrophobic interaction column

SEC chromatogram demonstrates the elution of alpha synuclein with dominant peak at 14.5 mL retention volume. A smaller protein eluted at a retention volume of 20 mL, representing a contaminant. The fractions from F6 to F14 was analyzed via of the SDS-PAGE gel to assess the purity. The resulting SDS-PAGE gel Figure 4.6 demonstrated the purity of alpha synuclein from SEC column was greater than 96% purity.

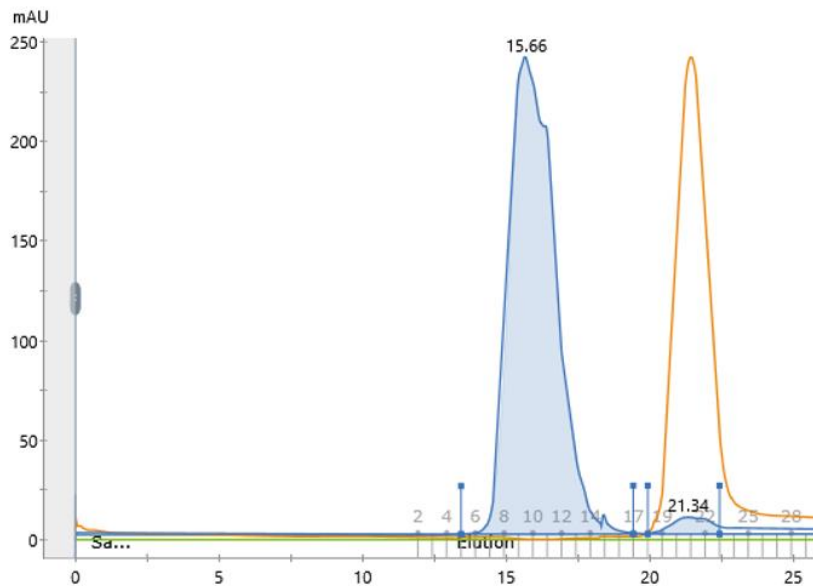


Figure 4.5 size exclusion chromatography of alpha synuclein

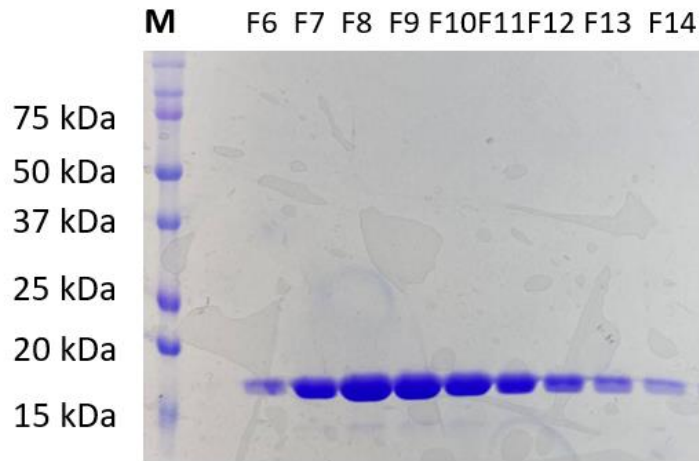


Figure 4.6 12.5% SDS-PAGE of fractions from SEC column

Ion exchange chromatogram demonstrated that Tau eluted out at second peak with 20% buffer B step gradient. The fraction was mixed with SDS sample buffer and analyzed using SDS-PAGE gel. The SDS-PAGE gel Figure 4.2 demonstrated the purity of Tau from Ion exchange column was approximately around 80% purity. The most dominant band around 110 kDa represented Tau, while there were multiply bands around 70kDa represented the impurity protein could be clearly observed. The fractions were collected and concentrated for the size exclusion column in order to reach a purity over 95% for downstream experiments.

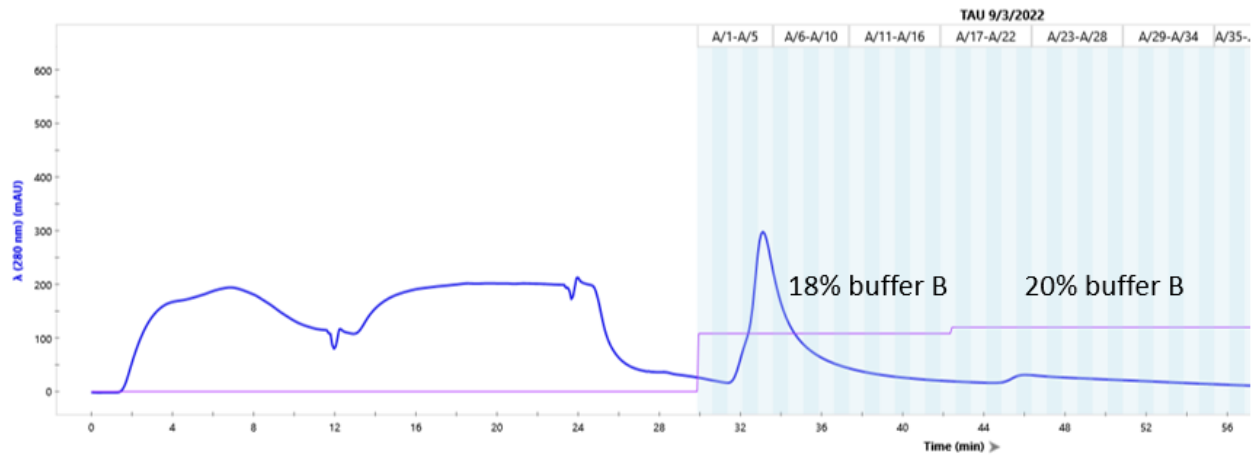


Figure 4.7 Ion exchange chromatography of Tau

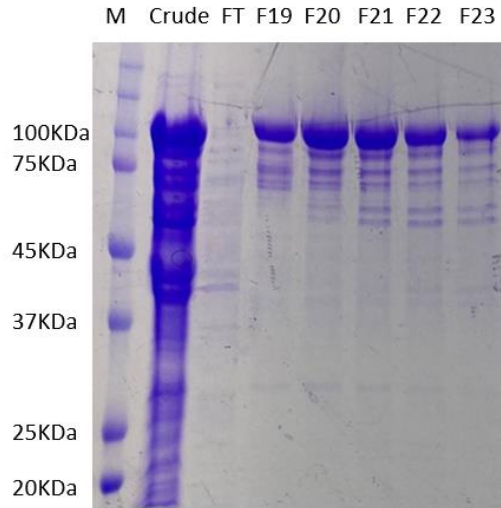


Figure 4.8 10% SDS-PAGE of fractions from ion exchange column

SEC chromatogram demonstrates the elution of Tau with the most dominant peak at 12.5 mL retention volume. Other peaks shown represented the elution of contaminant protein. The fractions from F19 to F26 was assessed the purity through the SDS-PAGE analysis. The SDS-PAGE gel Figure 4.6 demonstrated the purity of Tau from SEC column was higher than 95% purity.

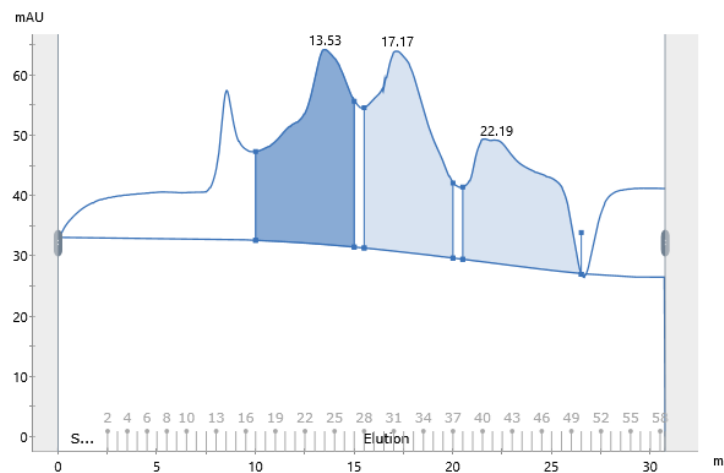


Figure 4.9 size exclusion chromatogram of Tau

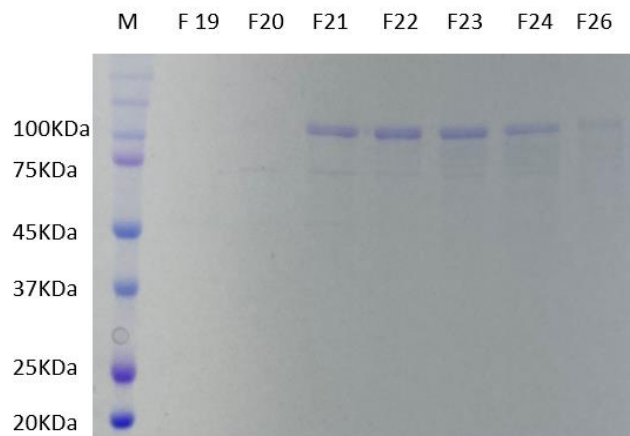


Figure 4.10 10% SDS-PAGE of fractions from size exclusion column

It is worth noting that both Hsp27 WT and triple serine mutant proteins display similar elution profiles in the ion exchange chromatogram. The fraction from F17 to F25 was mixed with SDS sample buffer and analysis through the SDS-PAGE electrophoresis. The SDS-PAGE gel Figure 4.11 demonstrated the purity of Hsp27 triple serine mutant from Ion exchange column was proximately around 90% purity. The most dominant band around 27 kDa represented Hsp27 protein.

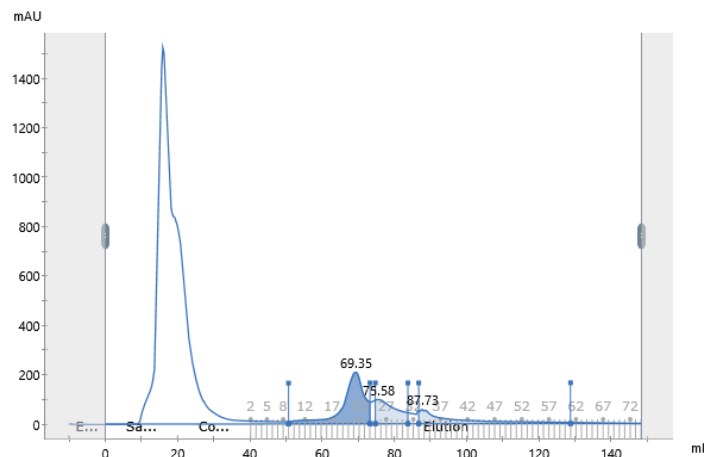


Figure 4.11 Ion exchange chromatogram of Hsp27

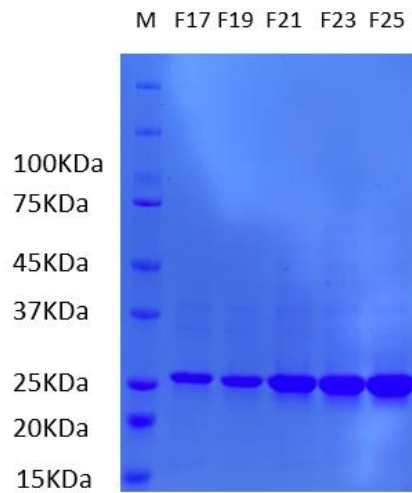


Figure 4.12 10% SDS-PAGE of fractions from ion exchange column

Size exclusion chromatogram demonstrated the elution profile of Hsp27 WT and triple serine mutant. The Hsp27 was observed to elute at 12 mL retention volume, while Hsp27 triple serine mutant eluted at 15 mL retention volume. The fraction was mixed with SDS sample buffer and analyzed use SDS-PAGE gel. The SDS-PAGE gel Figure 4.11 demonstrated the purity of Hsp27 from Size exclusion chromatograph was proximately around 95% purity, with the most dominant band around 27 kDa represented Hsp27 protein.

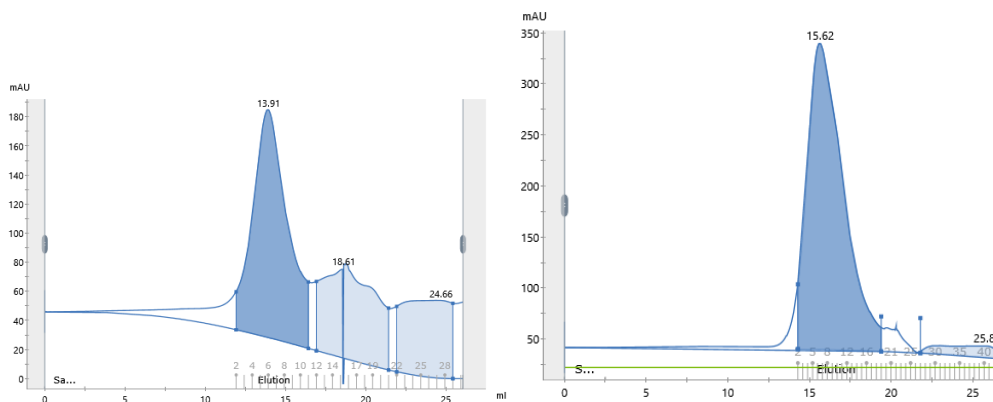


Figure 4.13 Comparison of size exclusion chromatography of Hsp27 WT with Hsp27 triple serine mutant

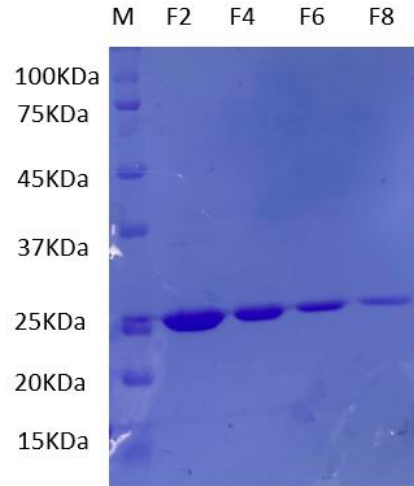


Figure 4.14 12.5% SDS-PAGE of fractions from size exclusion column

4.4 DISCUSSION

Through the combination of different types of chromatography, all the target proteins were able to reach high purity ready for structural and functional study. Alpha synuclein achieved a purity of over 98%, with a yield of approximately 8.5mg protein per liter of cell culture. There was no protease induced degradation or aggregation observed during the entire purification process. The purified alpha synuclein was ready for the fiber formation assay. The purity of Tau was 95% purity which was slightly lower compared to the alpha synuclein. Based on preliminary expression optimization, induction performed at 30 °C with 1mM IPTG was able to reach highest yield. Around 2mg Tau was able to be obtained from each liter cell culture. The final purity of Hsp27 WT and Hsp27 triple serine mutant was both above 95%. Approximately 9mg of each protein was able to be extracted from each liter cell culture. The almost identical elution profile demonstrated from Ion exchange chromatogram indicated that the similar surface charge profile of Hsp27 WT and Hsp27 triple serine mutant. However, the size exclusion chromatogram depicted the significant size difference between two proteins. The notable peak shift could be observed in the size exclusion chromatogram. In size exclusion chromatography,

the order of elution is determined by the overall size and shape of the protein complex. The larger protein will elute earlier than the smaller one. The constitutive active mutant mutated contained three aspartic acids, which mimicked the natural phosphorylation of Hsp27 WT. Phosphorylation of Hsp27 WT with MAPKAPK2 would cause disassembly of larger oligomer complex into the dimeric complexes. The encoded protein from Hsp27 constitutively active gene that could only form homogenous dimer not the natural large oligomer. The preliminary Hsp27 activity assay demonstrated the almost identical chaperone activity for inhibition of natural substrate protein aggregation for phosphorylated Hsp27 WT and Hsp27 constitutively active serine mutant.

Overall, based on the established purification protocol, homogenous and stable protein was able to be obtained from cell lysate for all the target of proteins in this study.

Chapter 5: Structural and Biophysical Characterization

5.1 BACKGROUND

Protein enzymatic function is highly correlated with its three-dimensional structure. In order to fully understand its activity properties, structural or biophysical characterization is frequently employed to investigate protein functional domains. The majority of analysis is dependent on investigation of protein folding profile or secondary structure which is directly associated to its unique function. [68] Various of structure motifs such as Zinc finger, Rossmann fold are identified in different proteins which participate in diverse metabolic pathways to maintain cellular homeostasis.[69] The interpretation of protein active site has been demonstrated the essential step for the advancement of modern drug discovery. The novel strategies identified the shape and thermodynamics profile of the protein active site is considered one of the most critical criteria for design the inhibitory ligand. Understanding the active sites of enzyme allows researchers to advance robust and highly specific drug inhibitors that can target disease related proteins while minimizing detrimental effects on normal cells. Thus, protein active site interpretation is a fundamental perspective of modern drug discovery, which plays a vital role in the advancement of novel treatments for numerous diseases.[70]

Dynamic light scattering (DLS) is a versatile laser-based approach to reveal size distribution profile of molecular complex in solution. Through accurate quantification of the Brownian motion of small particles in solution, the hydrodynamic radius profile can be determined. The Stokes-Einstein equation is applied to report the hydrodynamic radius of the particle which is proportional to its diffusion coefficients. DLS is frequently exploited to characterize the protein dispersion effect with the variation of pH, temperature, or salt concentration.[71] Thus, this approach is broadly utilized in thermos on ionic strength induced

protein conformational change research. The traditional DLS instrument is primarily composed of two parts, the laser beam and scatter signal detector as shown in Figure 5.1. The sample is placed in cuvette and illuminated with a laser beam. The corrected scatter signal is captured through the high sensitivity detector.[72]

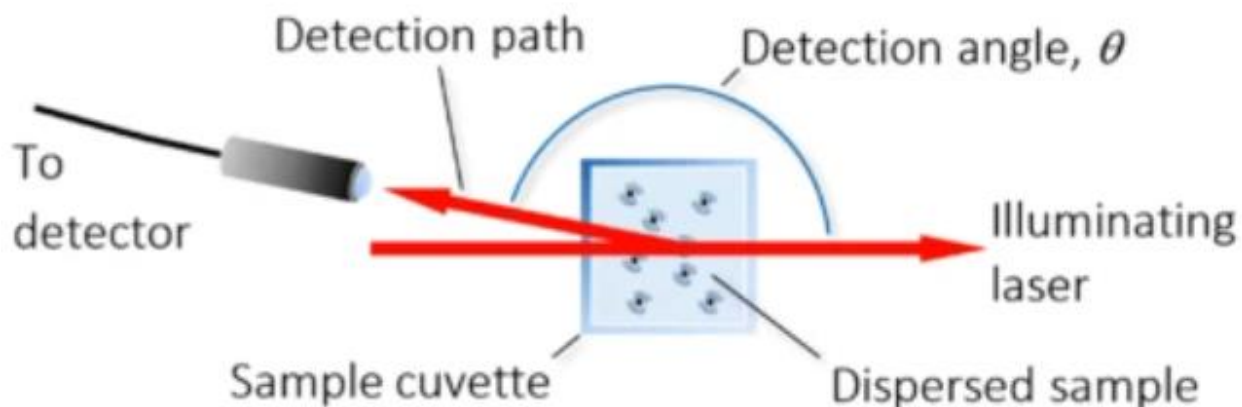


Figure5.1: Traditional Dynamic light scattering schematic diagram [73]

The detector will demonstrate the rate of fluctuation in light intensity which corresponds to the rate of diffusion of the particles. Smaller particle is able to diffuse much faster, which causes higher light intensity than the larger particle. [74] Due to the less time consuming and straightforward sample preparation, DLS is commonly conjugated with SEC or other techniques for early-stage structural characterization.

In order to achieve comprehensive understand of the protein structural information, it is crucial to obtain high atomic resolution structure. X-ray crystallography has been the most dominant structure investigation technique for several decades. The process involves purifying a high concentration of the protein of interest and crystallizing it. The crystals are then subjected to a high-energy X-ray beam, and the diffraction pattern reveals symmetry information and diffraction spots, which can be used to calculate the electron density map. With the appropriate

sample crystallization and data processing, the final resolution of macromolecular can higher than 3 Å. [75,76] While, the primary obstacle of X-ray crystallography is the time-consuming protein crystallization process which is still not entirely clear. To purify high quality and homogenous protein sample is the quintessential process for crystallization. Furthermore, a great deal of elements such as temperature, pH environment, ionic strength and presence of additives must be considered in order to generate the crystal as well.[77] Even though tremendous effort and time has been invested in this step, protein crystallization is still not guaranteed for certain type of protein such as intrinsic disordered protein. The common approach to execute structural investigation of intrinsic disordered protein is through cleavage of the intrinsic disordered domain to reveal the structure information of central well-defined domain. While numerous research have been demonstrated the drastic enzymatic activity change of truncation mutant compared with wild type full length disordered protein, which indicates the significance of intrinsic terminus in terms of modulation interaction with natural substrates.

The revolution of sample preparation, data processing and direct detection camera enables researchers to obtain near atomic resolution micromolecular complex with Cryo-electron microscope.[78] Unlike the traditional light microscope which utilizes photons for the source of radiation, the electron serves as imaging source for the electron microscope.[79] The accelerated electrons pass through the specimen in the near vacuum column. Then the scattered electrons converged by electromagnetic lens are able to be captured by the image plane. While, both near vacuum environments and high energy electrons is able to completely denature the biological samples. Thus, protein sample must be preserved before imaging via the electron microscopy. Plunge freezing is the process to freeze biological sample through submerging in the cryogen, which preserve protein in their near native conformation. The liquid ethane or propane are the

typical cryogen used for plunge freeze. Due to the extremely rapid freezing process, the bulky ice crystals are not able to form and the samples is embedded in the amorphous ice which is able to protect protein from electron radiation. This approach has been considered as the golden standard for Cryo-EM sample preparation.[80] Currently, the commercially available semi-automatic Vitrobot or manual blunge freeze workstation is able to accurately and reproducibly prepare the high-quality specimen for the Cryo-EM 3D reconstruction.

Negative stain is an alternative approach for transmission electron microscope sample imaging. Through staining specimen with contrast enhancing heavy metal reagent, this technique enables straightforward and less time-consuming initial data screening. Negative staining is frequently applied to rapid assess biological sample stability and homogeneity before targeting for cyro sample preparation.[81] The conventional contrast enhancing staining reagent is uranyl acetate, uranyl formate. These reagents usually are prepared in MilliQ degassed water to reach 1% to 2% final working concentration. [82] For negative stain, the biological sample is absorbed onto the surface of grid and blotted with compatible filter paper. The heavy metal reagent then stain the grid to promote the contrast when imaging. Compared with cryo frozen sample, the negative stain sample is able to generate relative higher contrast. The high contrast is contributed from the difference of electron dense between biological sample and surrounding stain reagent. The background appears darker primarily because stain is able to scatter more electrons. While the target of protein will show in lighter arear due to less electron scattering.[83] One of the major drawbacks of this approach is the low working pH of heavy metal stain reagent, which will potentially lead to fragile protein complex disassembled. Certain types of protein must skip the negative stain initial screening and directly optimize with cryo sample. If significant presence

of aggregation or partially denatured complex in the negative stain image was observed, the protein extraction and purification process had to be reoptimized accordingly.

5.2 MATERIAL AND METHOD

5.2.1 Alpha Synuclein Aggregation Assay

250 μ L of 300 μ M purified alpha synuclein was diluted in aggregation buffer (20mM Tris-base and 150mM KCl pH=7.5). All samples were loaded into 500 μ l Eppendorf tube and sealed with parafilm. The aggregation reaction was performed at 37 °C with constant agitation at 700 rpm for 160 hours. The aggregation product was stored in 4°C for short term storage. Twenty microliters of α -synuclein were obtained directly from the aggregation assay and diluted 1:4 with dH₂O. Three microliter samples were incubated on glow-discharged carbon-coated copper grides for 15s. Then 2% uranyl acetate was applied to stain the samples twice followed by 2% methylamine tungstate staining. The grid was imaged on the JOEL JEM 3200FS transmission electron microscope. Images were acquired at a magnification of 100,000x with a 0.3 second exposure in a Gatan® CCD camera.

5.2.2 Tau Fiber Formation Assay

Tau proteins (3.0 mg/ml) were incubated with heparin (400 μ g/mL) in 30 mM HEPES, 100 mM NaCl, pH 7.2, 1 mM AEBSF, and 4 mM TCEP at 37°C with constant agitation at 220 RPM for 95 hours. Twenty microliters of Tau were obtained directly from the aggregation assay and diluted 1:2 with dH₂O. Three microliter samples were incubated on glow-discharged carbon-coated copper grides for 10s. Then 2% uranyl acetate was applied to stain the samples twice followed by 2% methylamine tungstate staining. The grid was imaged on the JOEL JEM 3200FS transmission electron microscope.

5.2.3 DLS Measurement

All the dynamic light scattering measurements were executed with Malvern Zetasizer instrument. The protein sample were diluted to 0.3 mg/mL with desired SEC buffer. For the DLS measurement of Hsp27 WT and Hsp27 constitutive active mutant, the DLS instrument was preequilibrated at 25 for 1 minute. Subsequently, 50 μ L of diluted sample was transferred in disposable cuvette and equilibrated at 25 °C for 1 minute. The preset measurement program was used to perform triplicate measurement automatically.

5.2.4 Hsp27 Fiber Complex Assemble Assay

2 mg/mL Hsp27 triple serine mutant were incubated with 3 mg/mL tau fiber and 3 mg/mL alpha synuclein fiber at 25 °C for 1 hour. The resulting reaction was centrifuged at 14,000xg with benchtop centrifuge at room temperature for 5 minutes. The supernatant was discarded and precipitated pellet was resuspended. The 5 μ L supernatant and pellet was mixed with SDS sample buffer and run at 10% SDS-PAGE gel at 220 V for 45 minutes. Three microliters of resuspended pellet were incubated on glow-discharged carbon-coated copper grides for 10s. Then 2% uranyl acetate was applied to stain the samples twice followed by 2% methylamine tungstate staining. The grid was imaged on the JOEL JEM 3200FS transmission electron microscope.

5.3 RESULT

The negative stain image acquired at 100,000 magnifications depicted the final alpha synuclein fiber formation product Figure 5.1. The image revealed individual well separated fibers, which displayed two major conformations, implied the rod shape and twister fiber, consistent with previous research.[84] The width of the individual fiber is around 10nm.

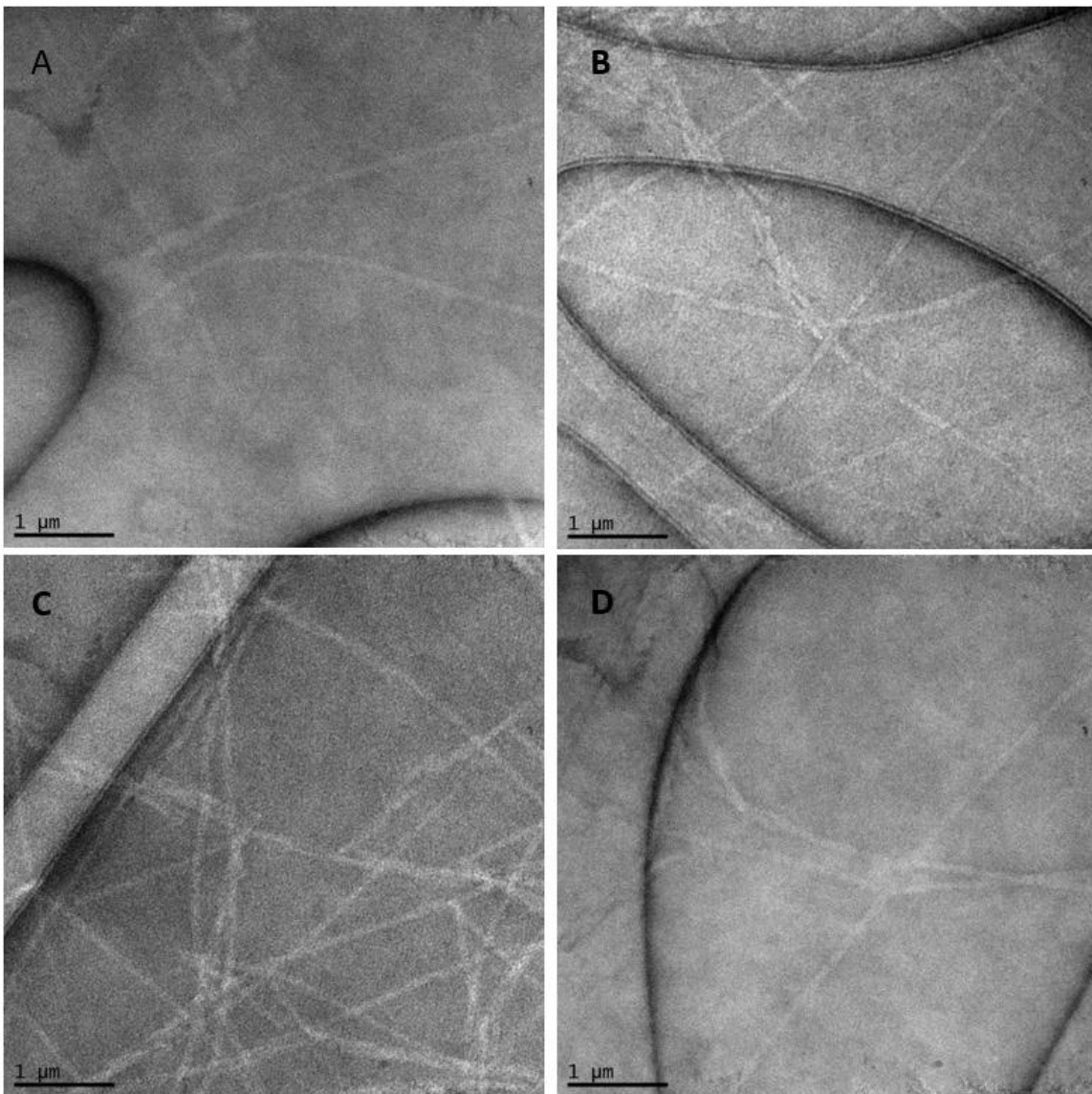


Figure 5.2 Negative stain image of alpha synuclein fiber

The negative stain image, acquired at 100,000 magnifications demonstrated the heparin induced Tau filament formation product as shown in Figure 5.2. The image depicted individual well separated Tau fiber. The snake like and hose like complex represent the two conformations of Tau fiber that have been described from preliminary research.[85] The width of the individual fiber is around 4nm.

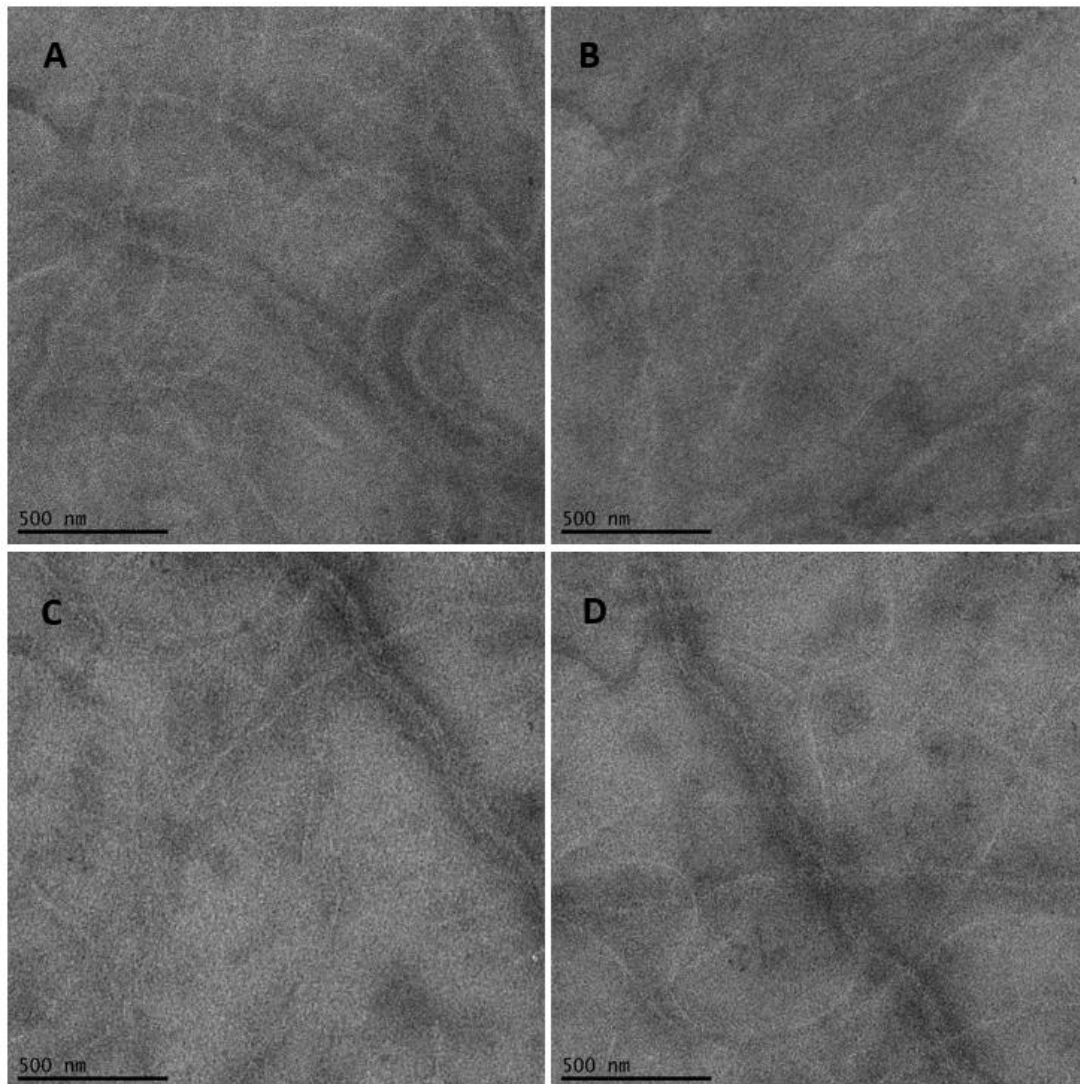


Figure 5.3 Negative stain image of heparin induced Tau fiber.

The dynamic light scattering (DLS) results provide valuable insights into the average size of Hsp27 constitutively active triple serine mutant and Hsp27 WT. The green curve corresponds to the Hsp27 triple serine mutant with the average size of 7.5nm while the red curve represented Hsp27 WT indicated the average size 13nm. Notably, the clear peak shift could be observed, which indicated the homogenous dimer of Hsp27 triple serine mutant.

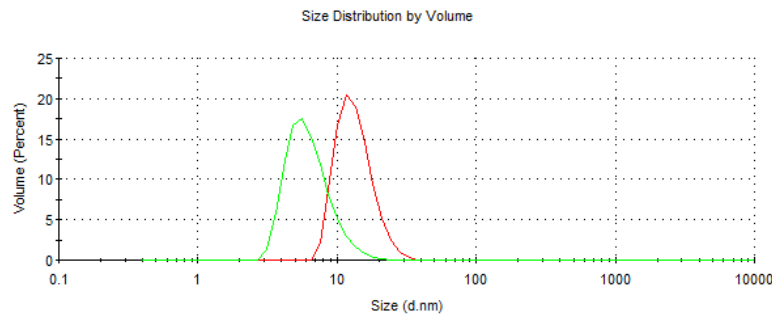


Figure 5.4 DLS analysis of Hsp27 triple serine mutant and Hsp27 WT

The SDS-PAGE analysis demonstrated the co-sedimentation assay result with the first line representing the supernatant sample and the second line represented the resuspended pellet. The top band represented the intact alpha synuclein fiber, which was unable to enter the resolving gel. The dominant band around 27 kDa in both first and second line was indicative of Hsp27 triple serine mutant. Additionally, the band at around 14.5 kDa was observed, which represented the alpha synuclein monomer.

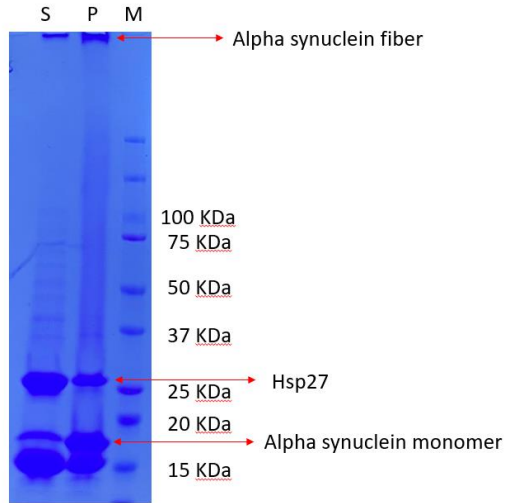


Figure 5.5 SDS-PAGE of alpha synuclein and Hsp27 triple serine mutant co-sedimentation assay

5.4 DISCUSSION

The negative stain image clearly provided visualization of the mature alpha synuclein fiber morphology with the rod and twist shapes being the most prevalent conformation. Based on the fiber growth conditions optimization, the condition outlined in the methods section led to the formation of well separated fiber, enable the downstream Hsp27 binding assay. Compared with alpha synuclein fiber, the morphology of Tau fiber exhibited distinct difference. There were four conformations of fiber observed from negative stain image, which has been illustrated from previous work.[86] The most dominant conformation was snake like shape fiber. The width of snake morphology fiber was estimated 4nm. Furthermore, approximately 10% of Tau fiber was in hose shape. The sigmoid hose fiber was clearly wider and shorter than the snake shape fiber. Even though the morphology of recombinant tau fiber was observed quite similar to the fiber extracted from brain sample, the high-resolution structures revealed the ineligibile difference between two types of the fibers. Overall, we were able to obtain well separated alpha synuclein fiber and tau fiber, which was the prerequisite for the helical reconstruction.

Under physiological condition, Hsp27 WT forms a large polydisperse oligomer. Hsp27 WT phosphorylated via MAPKAPK2 is able to lead large oligomer to dissociate to dimeric complex, but a great deal of small oligomer was still able to be observed under negative stain image. The polydispersity of the phosphorylated Hsp27 causes it unfeasible to reach high resolution with cryo-EM reconstruction. The triple serine mutant which is dominant in dimeric conformation is frequently applied to mimic Hsp27 stress induced phosphorylation. Preliminary research has suggested that the chaperone activity was similar to the phosphorylated Hsp27.[87] Thus, Hsp27 triple serine mutant was exploited in this study. The DLS analysis demonstrated the significant size difference between Hsp27 WT and Hsp27 triple serine mutant. The sharp and narrow peak indicated the monodispersed property of Hsp27 mutant.

Even though Hsp27 has been demonstrated to bind with alpha synuclein to inhibit its aggregation, whether Hsp27 is able to form complex with alpha synuclein fiber still needs to be

investigated. Co-sedimentation assay were employed to verify the competent of Hsp27 dimer to bind with alpha synuclein fiber to generate a stable complex. The SDS-PAGE analysis depicted the protein distribution after centrifugation. The majority of alpha synuclein fiber precipitated in the pellet as shown in the second wells of Figure 5.4. The SDS sample buffer insoluble alpha synuclein fiber remained in the top part of the resolving gel. The co-sedimentation of Hsp27 and alpha synuclein fiber could be clearly observed on the SDS-PAGE gel. The residual Hsp27 shown in the supernatant indicated that the excess amount of Hsp27 was applied for the complex assemble. For future study, the final concentration of Hsp27 can be optimized accordingly.

Due to intrinsic disorder of Hsp27 N terminus, the high atomic resolution still remains elusive. Neither cryo-EM or X-ray crystallography was unfeasible to reveal the structure information of N terminus of Hsp27. Preliminary co-sedimentation assay and fluorescence experiment suggested that the dimeric Hsp27 was able to bind to the alpha synuclein and Tau fiber via N terminus, which temporarily locked disordered domain to form well defined, ordered structure. Even though the size of dimeric Hsp27 approximately 54 kDa which still below the detection limit of robust digital detect camera, the reconstruction of entire fiber-Hsp27 complex was able to show the high-resolution structure of whole Hsp27 complex.

5.5 FUTURE DIRECTION

It is critical to optimize the conditions for the co-sedimentation assay to ensure that the interaction between Tau fiber and Hsp27 mutant is highly stable. The different protein concentrations and buffer conditions need to be investigated to find the optimal conditions for complex formation. Once the optimal assemble conditions have been determined, negative stain screening can be exploited to ensure that the fiber-Hsp27 complex is well-separated and suitable for cryo-EM imaging. Cryo-EM reconstruction will reveal high-resolution structural information about the Tau fiber-Hsp27 complex, which will aid to elucidate the fundamental mechanism of interaction between Hsp27 to neurodegenerative disease related protein.

References

1. Vabulas, R.M., Raychaudhuri, S., Hayer-Hartl, M., Hartl, F.U., 2010. Protein Folding in the Cytoplasm and the Heat Shock Response. *Cold Spring Harbor Perspectives in Biology*, a004390–a004390. doi:10.1101/cshperspect.a004390
2. Richter K., Haslbeck M., and Buchner J. (2010) The heat shock response: life on the verge of death. *Mol. Cell* 40, 253–266 10.1016/j.molcel.2010.10.006
3. Anfinsen CB. Principles that govern the folding of protein chains. *Science*. 1973;181:223–30.
4. Shakhnovich E. (2006). Protein folding thermodynamics and dynamics: where physics, chemistry, and biology meet. *Chemical reviews*, 106(5), 1559–1588. <https://doi.org/10.1021/cr040425u>
5. Dunker, A. K., Silman, I., Uversky, V. N. & Sussman, J. L. Function and structure of inherently disordered proteins. *Curr. Opin. Struct. Biol.* 18, 756–764 (2008).
6. Richter K., Haslbeck M., and Buchner J. (2010) The heat shock response: life on the verge of death. *Mol. Cell* 40, 253–266 10.1016/j.molcel.2010.10.006
7. Frydman, J., Nimmesgern, E., Ohtsuka, K. & Hartl, F. U. Folding of nascent polypeptide chains in a high molecular mass assembly with molecular chaperones. *Nature* 370, 111–117 (1994).
8. Bakthisaran R, Tangirala R, Rao ChM. Small heat shock proteins: Role in cellular functions and pathology. *Biochim Biophys Acta*. 2015 Apr;1854(4):291-319. doi: 10.1016/j.bbapap.2014.12.019. Epub 2014 Dec 30. PMID: 25556000.
9. Kappé, G., Boelens, W. C., & de Jong, W. W. (2010). Why proteins without an alpha-crystallin domain should not be included in the human small heat shock protein family HSPB. *Cell stress & chaperones*, 15(4), 457–461. <https://doi.org/10.1007/s12192-009-0155-4>
10. Haslbeck, M., Weinkauff, S., & Buchner, J. (2019). Small heat shock proteins: Simplicity meets complexity. *The Journal of biological chemistry*, 294(6), 2121–2132. <https://doi.org/10.1074/jbc.REV118.002809>
11. Haslbeck M, Franzmann T, Weinfurter D, Buchner J. Some like it hot: the structure and function of small heat-shock proteins. *Nat Struct Mol Biol*. 2005 Oct;12(10):842-6. Doi: 10.1038/nsmb993. PMID: 16205709.
12. Rajagopal, P., Liu, Y., Shi, L., Clouser, A. F., & Klevit, R. E. (2015). Structure of the α -crystallin domain from the redox-sensitive chaperone, HSPB1. *Journal of biomolecular NMR*, 63(2), 223–228. <https://doi.org/10.1007/s10858-015-9973-0>
13. Hochberg, G. K. A. et al. The structured core domain of B-crystallin can prevent amyloid fibrillation and associated toxicity. *Proc. Natl Acad. Sci. USA* 111, E1562–E1570 (2014).
14. Cohen, P. (2000). The regulation of protein function by multisite phosphorylation—a 25-year update. *Trends Biochem. Sci.* 25, 596–601. Doi: 10.1016/S0968-0004(00)01712-6
15. Webster, K. A. (2003). Serine phosphorylation and suppression of apoptosis by the small heat shock protein alphaB-crystallin. *Circ. Res.* 92, 130–132. Doi: 10.1161/01.RES.0000056967.51841.21
16. Tar K., Csontos C., Czikora I., Olah G., Ma S. F., Wadgaonkar R., et al. (2006). Role of protein phosphatase 2A in the regulation of endothelial cell cytoskeleton structure. *J. Cell. Biochem.* 98 931–953 10.1002/jcb.20829

17. Kostenko, S., and Moens, U. (2009). Heat shock protein 27 phosphorylation: kinases, phosphatases, functions, and pathology. *Cell. Mol. Life Sci.* 66, 3289–3307. Doi: 10.1007/s00018-009-0086-3
18. Kostenko, S., and Moens, U. (2009). Heat shock protein 27 phosphorylation: kinases, phosphatases, functions, and pathology. *Cell. Mol. Life Sci.* 66, 3289–3307. Doi: 10.1007/s00018-009-0086-3
19. Bakthisaran, R., Tangirala, R., and Rao Ch, M. (2015). Small heat shock proteins: role in cellular functions and pathology. *Biochim. Biophys. Acta* 1854, 291–319. Doi: 10.1016/j.bbapap.2014.12.019
20. Cox, D., Whiten, D. R., Brown, J., Horrocks, M. H., San Gil, R., Dobson, C. M., Klenerman, D., van Oijen, A. M., & Ecroyd, H. (2018). The small heat shock protein Hsp27 binds α -synuclein fibrils, preventing elongation and cytotoxicity. *The Journal of biological chemistry*, 293(12), 4486–4497. <https://doi.org/10.1074/jbc.M117.813865>
21. Laganowsky, A. et al. Crystal structures of truncated alphaA and alphaB crystallins reveal structural mechanisms of polydispersity important for eye lens function. *Protein Sci.* 19, 1031–1043 (2010)
22. Klevit, R. E. (2020). Peeking from behind the veil of enigma: emerging insights on small heat shock protein structure and function. *Cell Stress Chaperones* 25, 573–580. Doi: 10.1007/s12192-020-01092-2
23. Walsh DM, Selkoe DJ. Deciphering the molecular basis of memory failure in Alzheimer's disease. *Neuron* 2004;44:181–193.
24. Tau suppression in a neurodegenerative mouse model improves memory function. *Science*. 2005; 309 (16020737): 476-481 10.1126/science.1113694
25. Berriman J, Serpell LC, Oberg KA, Fink AL, Goedert M, Crowther RA. Tau filaments from human brain and from in vitro assembly of recombinant protein show cross-beta structure. *Proc Natl Acad Sci U S A*. 2003 Jul 22;100(15):9034-8. Doi: 10.1073/pnas.1530287100.
26. Goedert M, Spillantini MG, Jakes R, Rutherford DC, Crowther RA (1989) Multiple isoforms of human microtubule-associated protein tau: sequences and localization in neurofibrillary tangles of Alzheimer's disease *Neuron* 3:519–526. [https://doi.org/10.1016/0896-6273\(89\)90210-9](https://doi.org/10.1016/0896-6273(89)90210-9)
27. Ramkumar, A., Jong, B. Y., and Ori-McKenney, K. M. (2018). ReMAPping the microtubule landscape: how phosphorylation dictates the activities of microtubule-associated proteins. *Dev. Dyn.* 247, 138–155. doi: 10.1002/dvdy.24599
28. Hernandez F, Perez M, Lucas JJ, and Avila J. Are intracellular paired helical filaments (PHFs) from Alzheimer's disease toxic for a neuron? *Brain Aging* 1: 12–15, 2001.
29. Koss DJ, Jones G, Cranston A, Gardner H, Kanaan NM, Platt B (2016) Soluble pre-fibrillar tau and beta-amyloid species emerge in early human Alzheimer's disease and track disease progression and cognitive decline. *Acta Neuropathol* 132:875–895. <https://doi.org/10.1007/s00401-016-1632-3>
30. Fitzpatrick, A., Falcon, B., He, S. et al. Cryo-EM structures of tau filaments from Alzheimer's disease. *Nature* 547, 185–190 (2017). <https://doi.org/10.1038/nature23002>
31. Freilich, R., Betegon, M., Tse, E. et al. Competing protein-protein interactions regulate binding of Hsp27 to its client protein tau. *Nat Commun* 9, 4563 (2018). <https://doi.org/10.1038/s41467-018-07012-4>

32. Liu S, Ninan I, Antonova I, Battaglia F, Trinchese F, Narasanna A, et al. alpha-Synuclein produces a long-lasting increase in neurotransmitter release. *EMBO J.* (2004) 23:4506–16. doi: 10.1038/sj.emboj.7600451
33. Giasson BI, Murray IV, Trojanowski JQ, Lee VM A. hydrophobic stretch of 12 amino acid residues in the middle of alpha-synuclein is essential for filament assembly. *J Biol Chem.* (2001) 276:2380–6. doi: 10.1074/jbc.M008919200
34. Stefanis L. (2012). α -Synuclein in Parkinson's disease. *Cold Spring Harbor perspectives in medicine*, 2(2), a009399. <https://doi.org/10.1101/cshperspect.a009399>
35. Fortin D. L., Troyer M. D., Nakamura K., Kubo S., Anthony M. D. and Edwards R. H. (2004) Lipid rafts mediate the synaptic localization of alpha-synuclein. *J. Neurosci.* 24, 6715–6723.
36. Lou, X., Kim, J., Hawk, B. J., & Shin, Y. K. (2017). α -Synuclein may cross-bridge v-SNARE and acidic phospholipids to facilitate SNARE-dependent vesicle docking. *The Biochemical journal*, 474(12), 2039–2049. <https://doi.org/10.1042/BCJ20170200>
37. Liu, C., Zhao, Y., Xi, H., Jiang, J., Yu, Y., & Dong, W. (2021). The Membrane Interaction of Alpha-Synuclein. *Frontiers in cellular neuroscience*, 15, 633727. <https://doi.org/10.3389/fncel.2021.633727>
38. Cremades, N. et al. Direct observation of the interconversion of normal and toxic forms of alpha-synuclein. *Cell* 149, 1048–1059 (2012).
39. Flagmeier, P. et al. Mutations associated with familial Parkinson's disease alter the initiation and amplification steps of alpha-synuclein aggregation. *Proc. Natl Acad. Sci. USA* 113, 10328–10333 (2016).
40. Buell, A. K. et al. Solution conditions determine the relative importance of nucleation and growth processes in alpha-synuclein aggregation. *Proc. Natl Acad. Sci. USA* 111, 7671–7676 (2014).
41. Brundin, P. & Melki, R. Prying into the prion hypothesis for Parkinson's disease. *J. Neurosci.* 37, 9808–9818 (2017).
42. Cox, D., Whiten, D. R., Brown, J. W. P., Horrocks, M. H., San Gil, R., Dobson, C. M., Klenerman, D., van Oijen, A. M., & Ecroyd, H. (2018). The small heat shock protein Hsp27 binds α -synuclein fibrils, preventing elongation and cytotoxicity. *The Journal of biological chemistry*, 293(12), 4486–4497. <https://doi.org/10.1074/jbc.M117.813865>
43. Lessard JC. Molecular cloning. *Methods Enzymol.* 2013;529:85-98. doi: 10.1016/B978-0-12-418687-3.00007-0. PMID: 24011038.
44. Chang, D., Tram, K., Li, B. et al. Detection of DNA Amplicons of Polymerase Chain Reaction Using Litmus Test. *Sci Rep* 7, 3110 (2017). <https://doi.org/10.1038/s41598-017-03009-z>
45. Wang, W. and B.A. Malcolm, Two-stage PCR protocol allowing introduction of multiple mutations, deletions and insertions using QuikChange Site-Directed Mutagenesis. *Biotechniques*, 1999. 26(4): p. 680-2.
46. Jasmine E. Bird, Jon Marles-Wright, Andrea Giachino. A User's Guide to Golden Gate Cloning Methods and Standards. *ACS Synthetic Biology* 2022, 11 (11) , 3551-3563
47. Wilkinson A., Day J., Bowater R.. Bacterial DNA ligases. *Mol. Microbiol.* 2001; 40:1241–1248.
48. Pascal J.M., Tsodikov O.V., Hura G.L., Song W., Cotner E.A., Classen S., Tomkinson A.E., Tainer J.A., Ellenberger T.. A flexible interface between DNA ligase and PCNA

- supports conformational switching and efficient ligation of DNA. *Mol. Cell.* 2006; 24:279–291.
49. Sezonov, G., Joseleau-Petit, D., and D'Ari, R. (2007). *Escherichia coli* physiology in Luria-Bertani broth. *J. Bacteriol.* 189, 8746–8749. doi: 10.1128/JB.01368-07
 50. Chung, C.T., S.L. Niemela, and R.H. Miller, One-step preparation of competent *Escherichia coli*: transformation and storage of bacterial cells in the same solution. *Proceedings of the National Academy of Sciences*, 1989. 86(7): p. 2172-2175.
 51. Ford, T. J., & Way, J. C. (2015). Enhancement of *E. coli* acyl-CoA synthetase FadD activity on medium chain fatty acids. *PeerJ*, 3, e1040. <https://doi.org/10.7717/peerj.1040>
 52. Froger A, Hall JE. Transformation of plasmid DNA into *E. coli* using the heat shock method. *J Vis Exp.* 2007;(6):253. doi: 10.3791/253. Epub 2007 Aug 1. PMID: 18997900; PMCID: PMC2557105.
 53. Inoue H, Nojima H, Okayama H. High efficiency transformation of *Escherichia coli* with plasmids. *Gene.* 1990;96:23. doi: 10.1016/0378-1119(90)90336-P.
 54. Sorensen, H. P., and Mortensen, K. K. (2005). Advanced genetic strategies for recombinant protein expression in *Escherichia coli*. *J. Biotechnol.* 115, 113–128. doi: 10.1016/j.jbiotec.2004.08.004
 55. Müller-Hill, B. (1996b). “ β -Galactosidase, lac permease and transacetylase,” in *The Lac Operon: A Short History of a Genetic Paradigm*, ed. Berlin (New York, NY: Walter de Gruyter), 181.
 56. William Studier, F., et al., [6] Use of T7 RNA polymerase to direct expression of cloned genes. 1990, Elsevier. p. 60-89.
 57. Gomes, L., Monteiro, G., & Mergulhão, F. (2020). The Impact of IPTG Induction on Plasmid Stability and Heterologous Protein Expression by *Escherichia coli* Biofilms. *International journal of molecular sciences*, 21(2), 576. <https://doi.org/10.3390/ijms21020576>
 58. Shehadul Islam, M., Aryasomayajula, A., & Selvaganapathy, P. R. (2017). A Review on Macroscale and Microscale Cell Lysis Methods. *Micromachines*, 8(3), 83. <https://doi.org/10.3390/mi8030083>
 59. Primo ED, Otero LH, Ruiz F, Klinke S, Giordano W. The disruptive effect of lysozyme on the bacterial cell wall explored by an in-silico structural outlook. *Biochem Mol Biol Educ.* 2018 Jan;46(1):83-90. doi: 10.1002/bmb.21092. Epub 2017 Nov 13. PMID: 29131507.
 60. Blake, C. C. Koenig, D. F. Mair, G. A. North, A. C. Phillips, D. C., and Sarma, V. R. (1965) Structure of hen egg-white lysozyme. A three-dimensional Fourier synthesis at 2 Ångstrom resolution. *Nature* 206, 757–761.
 61. Johnson B.H., Hecht M.H. Cells by repeated cycles of freezing and thawing. *Biotechnology.* 1994;12:1357. doi: 10.1038/nbt1294-1357.
 62. Lazarus, R. A., & Wagener†, J. S. (2019). Recombinant Human Deoxyribonuclease I. *Pharmaceutical Biotechnology: Fundamentals and Applications*, 471–488. https://doi.org/10.1007/978-3-030-00710-2_22
 63. OXENBURGH, M., SNOSWELL, A. Use of Streptomycin in the Separation of Nucleic Acids from Protein in a Bacterial Extract. *Nature* 207, 1416–1417 (1965). <https://doi.org/10.1038/2071416a0>

64. Boyer, R. F. (1993) Separation and purification of biomolecules by chromatography, in *Modern Experimental Biochemistry*, Benjamin-Cummings, Redwood City, CA, pp. 90–102.
65. Jonas Lohr, Simon Baukmann, Jonathan Block, Marc Upmann, Antje C. Spieß, Understanding adsorption behavior of antiviral labyrinthopeptin peptides in anion exchange chromatography, *Journal of Chromatography A*, 10.1016/j.chroma.2023.463792, 1690, (463792), (2023).
66. J.C. Rea, G.T. Moreno, Y. Lou, D. Farnan, Validation of a pH gradient based ionexchange chromatography method for high-resolution monoclonal antibody charge variant separations, *J. Pharm. Biomed. Anal.* 54 (2011) 317–323.
67. Audain, E., Ramos, Y., Hermjakob, H., Flower, D. R., and Perez-Riverol, Y. (2016). Accurate Estimation of Isoelectric point of Protein and Peptide Based on Amino Acid Sequences. *Bioinformatics (Oxford, England)* 32 (6), 821–827. doi:10.1093/bioinformatics/btv674
68. Brange J., Langkjaer L., Havelund S., Vølund A. Chemical Stability of Insulin. 1. Hydrolytic Degradation During Storage of Pharmaceutical Preparations. *Pharm. Res.* 1992;9(6):715–726.
69. Hong, P., Koza, S., & Bouvier, E. S. (2012). Size-Exclusion Chromatography for the Analysis of Protein Biotherapeutics and their Aggregates. *Journal of liquid chromatography & related technologies*, 35(20), 2923–2950. <https://doi.org/10.1080/10826076.2012.743724>
70. Zhang C, Kim SH. Overview of structural genomics: from structure to function. *Curr Opin Chem Biol.* 2003;7:28–32.
71. Kinoshita K, Nakamura H. Protein informatics towards function identification. *Curr Opin Struct Biol.* 2003;13:396–400.
72. An J, Totrov M, Abagyan R. Pocketome via comprehensive identification and classification of ligand binding envelopes. *Mol Cell Proteomics.* 2005 Jun;4(6):752–61. doi: 10.1074/mcp.M400159-MCP200. Epub 2005 Mar 9. PMID: 15757999.
73. Bauer, K., Göbel, M., Schwab, M., Schermeyer, M. & Hubbuch, J. Concentration-dependent changes in apparent diffusion coefficients as indicator for colloidal stability of protein solutions. *Int. J. Pharm* 511, 276–287 (2016).
74. Malm, A.V., Corbett, J.C.W. Improved Dynamic Light Scattering using an adaptive and statistically driven time resolved treatment of correlation data. *Sci Rep* 9, 13519 (2019). <https://doi.org/10.1038/s41598-019-50077-4>
75. Bootz, A., Vogel, V., Schubert, D. & Kreutera, J. Comparison of scanning electron microscopy, dynamic light scattering and analytical ultracentrifugation for the sizing of poly(butyl cyanoacrylate) nanoparticles. *European Journal of Pharmaceutics and Biopharmaceutics* 57(2), 369–375 (2004).
76. Luft JR, Arakali SV, Kirisits J, et al. A macromolecular crystallization procedure employing diffusion cells of varying depths as reservoirs to tailor the time course of equilibration in hanging drop and sitting drop vapour diffusion and microdialysis experiments. *Journal of Applied Crystallography* 1994;27:443–53.
77. Wilson LJ, Bray TL, Suddath FL. Crystallization of proteins by dynamic control of evaporation. *Journal of Crystal Growth* 1991;110:142–7.
78. Carter CW, Carter CW. Protein crystallization using incomplete factorial experiments. *J Biol Chem* 1979;254:12219–23.

79. Milne, J. L., Borgnia, M. J., Bartesaghi, A., Tran, E. E., Earl, L. A., Schauder, D. M., Lengyel, J., Pierson, J., Patwardhan, A., & Subramaniam, S. (2013). Cryo-electron microscopy--a primer for the non-microscopist. *The FEBS journal*, 280(1), 28–45. <https://doi.org/10.1111/febs.12078>
80. Hurbain I, Sachse M. The future is cold: cryo-preparation methods for transmission electron microscopy of cells. *Biol Cell*. 2011;103:405–20.
81. Subramaniam S, Bartesaghi A, Liu J, Bennett AE, Sougrat R. Electron tomography of viruses. *Curr Opin Struct Biol*. 2007;17:596–602.
82. Burgess SA, Walker ML, Thirumurugan K, Trinick J, Knight PJ. Use of negative stain and single-particle image processing to explore dynamic properties of flexible macromolecules. *J Struct Biol*. 2004;147(3):247–258.
83. Scarff, C. A., Fuller, M. J. G., Thompson, R. F., & Iadanza, M. G. (2018). Variations on Negative Stain Electron Microscopy Methods: Tools for Tackling Challenging Systems. *Journal of visualized experiments : JoVE*, (132), 57199. <https://doi.org/10.3791/57199>
84. Ohi M, Li Y, Cheng Y, Walz T. Negative Staining and Image Classification - Powerful Tools in Modern Electron Microscopy. *Biol Proced Online*. 2004;6(1):23–34.
85. Li, B., Ge, P., Murray, K.A. et al. Cryo-EM of full-length α -synuclein reveals fibril polymorphs with a common structural kernel. *Nat Commun* 9, 3609 (2018). <https://doi.org/10.1038/s41467-018-05971-2>
86. Crowther RA. Straight and paired helical filaments in Alzheimer disease have a common structural unit. *PNAS*. 1991;88:2288–2292. doi: 10.1073/pnas.88.6.2288.
87. Jovceviski B., Kelly M. A., Rote A. P., Berg T., Gastall H. Y., Benesch J. L., Aquilina J. A., and Ecroyd H. (2015) Phosphomimics destabilize Hsp27 oligomeric assemblies and enhance chaperone activity. *Chem. Biol.* 22, 186–195 [10.1016/j.chembiol.2015.01.001](https://doi.org/10.1016/j.chembiol.2015.01.001)

Vita

Zhaobo Li was born and raised in Harbin, China. As a graduate student he joined the laboratory of Dr. Ricardo A. Bernal to conduct structure biology research to investigate neurodegenerative disease. During his time as a graduate student, Zhaobo enjoyed teaching several undergraduate level lab sections. He also presented his graduate research in several conferences.

Zhaobo currently lives in El Paso. He enjoys watching sports and movies. He feels incredibly fortunate to have Dr. Ricardo Bernal as his mentor and hopes to continue dedicate himself in the structure biology related research.

Contact Email: zhaobolim.d@gmail.com